

General relativistic effects on neutrino-driven wind from young, hot neutron star and the r-process nucleosynthesis

Kaori Otsuki¹

Division of Theoretical Astrophysics, National Astronomical Observatory, Mitaka, Tokyo 181-8588

Hideyuki Tagoshi

Department of Earth and Space Science, Osaka University, Toyonaka, Osaka 560-0043

Toshitaka Kajino^{2,3} and Shin-ya Wanajo

Division of Theoretical Astrophysics, National Astronomical Observatory, Mitaka, Tokyo 181-8588

ABSTRACT

Neutrino-driven wind from young hot neutron star, which is formed by supernova explosion, is the most promising candidate site for r-process nucleosynthesis. We study general relativistic effects on this wind in Schwarzschild geometry in order to look for suitable conditions for a successful r-process nucleosynthesis. It is quantitatively discussed that the general relativistic effects play a significant role in increasing entropy and decreasing dynamic time scale of the neutrino-driven wind. Exploring wide parameter region which determines the expansion dynamics of the wind, we find interesting physical conditions which lead to successful r-process nucleosynthesis. The conditions which we found realize in the neutrino-driven wind with very short dynamic time scale $\tau_{\text{dyn}} \sim 6$ ms and relatively low entropy $S \sim 140$. We carry out the α -process and r-process nucleosynthesis calculation on these conditions by the use of our single network code including over 3000 isotopes, and confirm quantitatively that the second and third r-process abundance peaks are produced in the neutrino-driven wind.

Subject headings:

¹Research Center for Nuclear Physics, Osaka University, Ibaraki, Osaka 560-0043

²Department of Astronomy, University of Tokyo, Hongo, Tokyo 113-0033

³Department of Astronomical Science, The Graduate University for Advanced Studies, Mitaka, Tokyo 181-8588

1. Introduction

The r-process is a nucleosynthesis process to produce elements heavier than iron (Burbidge et al. 1957). They occupy nearly half of the massive nuclear species, and show typical abundance peaks around nuclear masses $A=80$, 130 and 195, whose neutron numbers are slightly smaller than the magic numbers $N=50$, 82 and 126, respectively. This fact suggests that the r-process elements have completely different origin from the s-process elements whose abundance peaks are located just on the neutron magic numbers. The r-process elements are presumed to be produced in an explosive environment with short time scale and high entropy, where intensive flux of free neutrons are absorbed by seed elements successively to form the nuclear reaction flow on extremely unstable nuclei in neutron-rich side. Recent progress in the studies of nuclear physics of unstable nuclei has made it possible to simulate the r-process nucleosynthesis by the use of accumulated knowledge on nuclear masses and beta half-lives of several critical radioactive elements.

The studies of r-process elements make another impact on the cosmic age problem, that is the age of the Universe to be known from cosmological constants and the age of the oldest globular cluster conflict with each other. A typical r-process element, thorium, has been detected recently in very metal-deficient stars, providing independent method to estimate the age of the Milky Way Galaxy (Sneden et al. 1996). Since thorium has half-life of 14 Gyr, the observed abundance relative to the other stable elements is used as a chronometer dating the age of the Galaxy. To study the origin of the r-process elements is thus important and even critical in cosmology and astronomy of Galactic chemical evolution as well as nuclear physics of unstable nuclei. Unfortunately, however, astrophysical site of the r-process nucleosynthesis has been poorly known, although several candidate sites are proposed and being investigated theoretically.

Neutrino-driven wind, which is our object to study in this article, is thought to be one of the most promising candidates for the r-process nucleosynthesis. It is generally believed that a neutron star is formed as the remnant of gravitational core collapse of Type II, Ib or Ic supernovae. The hot neutron star just born releases most of its energy as neutrinos during Kelvin-Helmholtz cooling phase, and these neutrino drive matter outflow from the surface. This outflow is called neutrino-driven wind. Many theoretical stud-

ies of neutrino-driven wind followed the successful detection of energetic neutrinos from SN1987A, which raised the possibility of finding the r-process nucleosynthesis in this wind.

Although there are several numerical simulations of the neutrino-driven wind, results are very different from one another, depending on models and methods adopted in literature (Woosley et al. 1994, Witt, Janka, & Takahashi 1994, Takahashi, Witt, & Janka 1994). A benchmark study of numerical simulation by Wilson and his collaborators (Woosley et al. 1994) can successfully explain the solar system r-process abundances, but the others (Witt, Janka, & Takahashi 1994, Takahashi, Witt, & Janka 1994) can not reproduce their result. Qian and Woosley (1996) tried to work out this discrepancy using approximate methods to solve the spherically symmetric, steady state flow in the Newtonian framework.

They could not find suitable condition for the r-process nucleosynthesis, and they suggested in a post-Newtonian calculation that general relativistic effects may improve thermodynamic condition for the r-process nucleosynthesis. Cardall and Fuller (1997) adopted similar approximate methods in general relativistic framework and obtained short dynamic time scale of the expansion and large entropy, which is in reasonable agreement with the result in post-Newtonian approximation adopted by Qian and Woosley (1996). They did not remark quantitatively, however, what kind of specific effect among several general relativistic effects is responsible for this change.

Since the wind blows near the surface of the neutron star, it is needed to study expansion dynamics of neutrino-driven wind in general relativity. The first purpose of this paper is to quantitatively make clear the effects of general relativity by adopting fully general relativistic framework. Although we assume only spherical steady-state flow of the neutrino-driven wind, we do not adopt approximate methods as in several previous studies. We try to extract as general properties as possible of the wind in manners independent of supernova models so that they are to be compared with expansion of different object like accretion disk of binary neutron star merger (Symbalisty & Schramm 1982) or sub-critical small mass neutron star (Sumiyoshi et al. 1998), which is induced by intense neutrino burst. The second purpose is to look for suitable conditions for the r-process. There are key quantities in order to explain the so-

lar system r-process abundances. They are the mass outflow rate, \dot{M} , the dynamic time scale of the expansion, τ_{dyn} , the entropy, S , and the electron fraction, Y_e . The third purpose of this paper is to make clear how these thermodynamic and hydrodynamic quantities affect the r-process nucleosynthesis by carrying out the nucleosynthesis calculation numerically.

In the next section we explain our theoretical models of neutrino-driven wind. We introduce basic equations to describe the dynamics of the wind in the Schwarzschild geometry. Boundary conditions and adopted parameters for solving these equations are presented in this section. Numerical results are shown in section 3, where the effects of general relativity are studied in detail. We also investigate the dependence of the key physical quantities like τ_{dyn} and S on the neutron star mass, radius, and neutrino luminosity in order to look for the conditions of the neutrino-driven wind which is suitable for the r-process nucleosynthesis. Applying the result obtained in section 3, we carry out the nucleosynthesis calculation in section 4. The purpose of this section is to confirm quantitatively that the r-process elements are produced successfully in the wind having very short dynamic time scale with relatively low entropy. We finally summarize the results of this paper and present further discussions and outlook in section 5.

2. Models of neutrino-driven winds

2.1. Basic equations

Type II or Ib supernova explosion is one of the complex hydrodynamic process which needs careful theoretical studies of the convection associated with shock propagation. The time of our interest, however, is the later phase after the core bounce, at which the shock has already passed away to reach a radius about 10000 km and continuous mass outflow is installed from the surface of the neutron star. Recent three dimensional numerical simulation (Hillebrandt 1998) has indicated that the convection near the shock front does not grow as deep as that shown in two-dimensional numerical simulation and the hydrodynamic conditions behind the shock are more likely similar to those obtained in one-dimensional numerical simulation. Since Wilson's numerical simulation of SN1987A in Woosley et al. (1994) has shown that the neutrino-driven wind is adequately described by a steady state flow, we here adopt spherically symmetric and steady state wind, following the previous studies (Duncan, Shapiro, &

Wasserman 1986, Qian & Woosley 1996, Cardall & Fuller 1997). According to his numerical simulation, the neutrino luminosity L_ν changes slowly from about 10^{52} ergs/s to below 10^{51} ergs/s during ~ 10 s of the Kelvin-Helmholtz cooling phase of the neutron star. The properties of the protoneutron star, *i.e.* the mass M and radius R , also evolve slowly. We therefore take these quantities L_ν , M , and R as input parameters in order to describe more rapid evolution of the neutrino-driven wind.

The basic equations to describe the spherically symmetric and steady state winds in Schwarzschild geometry are given by (Shapiro & Teukolsky 1983)

$$\dot{M} = 4\pi r^2 \rho_b u, \quad (1)$$

$$u \frac{du}{dr} = \frac{1}{\rho_{\text{tot}} + P} \frac{dP}{dr} \left(1 + u^2 - \frac{2M}{r} \right) - \frac{M}{r^2}, \quad (2)$$

$$\dot{q} = u \left(\frac{d\varepsilon}{dr} - \frac{P}{\rho_b^2} \frac{d\rho_b}{dr} \right), \quad (3)$$

where \dot{M} is the mass outflow rate, r is the distance from the center of the neutron star, ρ_b is the baryon mass density, u is the radial component of the four velocity, $\rho_{\text{tot}} = \rho_b + \rho_b \varepsilon$ is total energy density, ε is the specific internal energy, P is the pressure, M is the mass of the neutron star, and \dot{q} is the net heating rate due to neutrino interactions with matter. We use the conventional units that the plank constant \hbar , the speed of light c , the Boltzmann constant k , and gravitational constant G , are taken to be unity. Since the neutrino-driven wind blows from the surface of the hot protoneutron star at high temperature $T \sim 5$ MeV and also the physics of the wind is mostly determined at $T \gtrsim 0.5$ MeV (Qian & Woosley 1996), the equations of state are approximately written as

$$P = \frac{11\pi^2}{180} T^4 + \frac{\rho_b}{m_N} T, \quad (4)$$

$$\varepsilon = \frac{11\pi^2}{60} \frac{T^4}{\rho_b} + \frac{3}{2} \frac{T}{m_N}, \quad (5)$$

where T is the temperature of the system, and m_N is the nucleon rest mass. We have assumed that the material in the wind consists of photons, relativistic electrons and positrons, and non-relativistic free nucleons.

The heating rate \dot{q} in Eq. (3) through the interactions between neutrinos and material takes the key to understand the dynamics of the neutrino-driven wind. Following Bethe (1993) and Qian and

Woosley (1994), we take account of the following five neutrino processes; neutrino and antineutrino absorption by free nucleons, neutrino and antineutrino scattering by electrons and positrons, and neutrino-antineutrino annihilation into electron-positron pair as the heating processes, and electron and positron capture by free nucleons, and electron-positron annihilation into neutrino-antineutrino pair as the cooling processes. We assume that neutrinos are emitted isotropically from the surface of the neutron star at the radius R , which proves to be a good approximation in recent numerical studies of the neutrino transfer (Yamada, Janka, & Suzuki 1999). In this paper, therefore, we make an assumption that the neutrinosphere radius is equal to the protoneutron star radius $R_\nu = R$. Since the neutrino trajectory is bent in the Schwarzschild geometry, the material in the wind sees neutrinos within the solid angle subtended by the neutrinosphere which is greater than the solid angle in the Newtonian geometry at the same coordinate radius. The bending effect of the neutrino trajectory increases the heating rate compared to Newtonian case. We have to take account of the redshift effect on the neutrino energy, too, which tends to decrease the heating rate.

The important heating rate is due to the neutrino and antineutrino absorption by free nucleons

$$\nu_e + n \rightarrow p + e^-, \quad (6)$$

$$\bar{\nu}_e + p \rightarrow n + e^+, \quad (7)$$

and it is given by

$$\begin{aligned} \dot{q}_1 &\approx 9.65 N_A [(1 - Y_e) L_{\nu_e, 51} \varepsilon_{\nu_e}^2 + Y_e L_{\bar{\nu}_e, 51} \varepsilon_{\bar{\nu}_e}^2] \\ &\times \frac{1 - g_1(r)}{R_{\nu 6}^2} \Phi(r)^6 \text{MeV s}^{-1} \text{g}^{-1}, \end{aligned} \quad (8)$$

where the first and second terms in the parenthesis are for the processes (6) and (7), respectively, ε_i is the energy in MeV defined by $\varepsilon_i = \sqrt{\langle E_i^3 \rangle / \langle E_i \rangle}$, and $\langle E_i^n \rangle$ denotes the n th energy moment of the neutrino ($i = \nu_e$) and antineutrino ($i = \bar{\nu}_e$) energy distribution, N_A is the Avogadro number, Y_e is the electron fraction, $L_{i, 51}$ is the individual neutrino or antineutrino luminosity in units of 10^{51} ergs/s, and $R_{\nu 6}$ is the neutrinosphere radius in units of 10^6 cm. In this equation, $1 - g_1(r)$ is the geometrical factor which represents the effect of bending neutrino trajectory, and $g_1(r)$ is given by

$$g_1(r) = \left(1 - \left(\frac{R_\nu}{r} \right)^2 \frac{1 - 2M/r}{1 - 2M/R_\nu} \right)^{1/2}, \quad (9)$$

where the function $(1 - 2M/r)/(1 - 2M/R_\nu)$ arises due to the Schwarzschild geometry, and unity should be substituted for this factor in the Newtonian geometry. We also define the redshift factor

$$\Phi(r) = \sqrt{\frac{1 - 2M/R_\nu}{1 - 2M/r}}, \quad (10)$$

in the Schwarzschild geometry, which is unity in the Newtonian geometry. We will discuss the effects of these general relativistic correction factors in the next section.

The second heating rate due to neutrino and antineutrino scattering by electrons and positrons plays equally important role. Neutrinos of all flavors can contribute to the scattering, and the heating rate is given by

$$\begin{aligned} \dot{q}_3 &\approx 2.17 N_A \frac{T_{\text{MeV}}^4}{\rho_8} \\ &\times \left(L_{\nu_e, 51} \epsilon_{\nu_e} + L_{\bar{\nu}_e, 51} \epsilon_{\bar{\nu}_e} + \frac{6}{7} L_{\nu_\mu, 51} \epsilon_{\nu_\mu} \right) \\ &\times \frac{1 - g_1(r)}{R_{\nu 6}^2} \Phi(r)^5 \text{MeV s}^{-1} \text{g}^{-1}, \end{aligned} \quad (11)$$

where $\epsilon_i = \langle E_i^2 \rangle / \langle E_i \rangle$ in MeV ($i = \nu_e, \bar{\nu}_e, \text{ and } \nu_\mu$), and we have assumed the same contribution from $\nu_\mu, \bar{\nu}_\mu, \nu_\tau$, and $\bar{\nu}_\tau$ fluxes. We take $\varepsilon_i^2 \simeq 1.14 \epsilon_i^2$ from the numerical studies by Qian and Woosley (1996).

The third heating rate due to neutrino-antineutrino pair annihilation into electron-positron pair is given by

$$\begin{aligned} \dot{q}_5 &\approx 12.0 N_A \\ &\times \left(L_{\nu_e, 51} L_{\bar{\nu}_e, 51} (\epsilon_{\nu_e} + \epsilon_{\bar{\nu}_e}) + \frac{6}{7} L_{\nu_\mu, 51}^2 \epsilon_{\nu_\mu} \right) \\ &\times \frac{g_2(r)}{\rho_8 R_{\nu 6}^4} \Phi(r)^9 \text{MeV s}^{-1} \text{g}^{-1}, \end{aligned} \quad (12)$$

where $g_2(r)$ is given by

$$g_2(r) = (1 - g_1(r))^4 (g_1(r)^2 + 4g_1(r) + 5). \quad (13)$$

The cooling rates which we included in the present calculations are for the inverse reactions of the two heating processes considered in Eqs. (8) and (12). The first cooling rate due to electron and positron captures by free nucleons, which are the inverse reactions of (6) and (7), is given by

$$\dot{q}_2 \approx 2.27 N_A T_{\text{MeV}}^6 \text{MeV s}^{-1} \text{g}^{-1}. \quad (14)$$

The second cooling rate due to electron-positron pair annihilation into neutrino-antineutrino pair of all flavors, which is the inverse reaction of Eq. (12), is given by

$$\dot{q}_4 \approx 0.144 N_A \frac{T_{\text{MeV}}^9}{\rho_8} \text{MeV s}^{-1} \text{g}^{-1}. \quad (15)$$

Combining the above five heating and cooling rates, we obtain the total net heating rate \dot{q}

$$\dot{q} = \dot{q}_1 - \dot{q}_2 + \dot{q}_3 - \dot{q}_4 + \dot{q}_5. \quad (16)$$

As we will discuss in the next section, the first three heating and cooling rates \dot{q}_1 , \dot{q}_2 , and \dot{q}_3 dominate over the other two contributions from \dot{q}_4 and \dot{q}_5 .

2.2. Boundary conditions and input parameters

We assume that the wind starts from the surface of the protoneutron star at the radius $r_i = R$ and the temperature T_i . Near the neutrinosphere and the neutron star surface, both heating (mostly \dot{q}_1) and cooling (mostly \dot{q}_2) processes almost balance with each other due to very efficient neutrino interactions with material. The system is thus in kinetic equilibrium (Barrows and Mazurek 1982) at high temperature and high density. The inner boundary temperature T_i is determined so that the net heating rate \dot{q} becomes zero at this radius. We have confirmed quantitatively that a small change in T_i does not influence the calculated thermodynamic and hydrodynamic quantities of the neutrino-driven wind very much. We give the density $\rho(r_i) = 10^{10} \text{ g/cm}^3$ at the inner boundary, which is taken from the result of Wilson's numerical simulation in Woosley et al. (1994).

The luminosity of each type of neutrino L_i ($i = \nu_e, \bar{\nu}_e, \nu_\mu, \bar{\nu}_\mu, \nu_\tau, \bar{\nu}_\tau$) is similar to one another and changes from about 10^{52} to 10^{50} ergs/s very slowly during ~ 10 s (Woosley et al. 1994). We therefore take a common neutrino luminosity L_ν as a constant input parameter. In the heating and cooling rates, however, we use the values of neutrino energies $\epsilon_{\nu_e} = 12 \text{ MeV}$, $\epsilon_{\bar{\nu}_e} = 22 \text{ MeV}$, and $\epsilon_\nu = \epsilon_{\bar{\nu}} = 34 \text{ MeV}$ for the other flavors at $r_i = R$ as in Qian & Woosley (1996). We take the neutron star mass as a constant input parameter ranging $1.2M_\odot \leq M \leq 2.0M_\odot$, too.

The mass outflow rate \dot{M} determines how much material is ejected by the neutrino-driven wind. In Eqs.(1)-(3), \dot{M} is taken to be a constant value to be determined by the following outer boundary condition. In any delayed explosion models of Type II su-

pernovae (Woosley et al. 1994, Wittl, Janka, & Takahashi 1994, Takahashi, Wittl, & Janka 1994), the shock wave moves away at the radius around 10000 km above the neutron star surface at times $1\text{s} \lesssim t$ after the core bounce. As we stated in the previous subsection, the neutrino-driven wind is described by a steady state flow fairly well between the neutron star surface and the shock. From this observation, a typical temperature at the location of the shock wave can be used as an outer boundary condition. We impose the boundary condition only for subsonic solutions by choosing the value of $\dot{M} < \dot{M}_{\text{crit}}$ so that $T = 0.1 \text{ MeV}$ at $r \simeq 10,000 \text{ km}$, where \dot{M}_{crit} is the critical value for supersonic solution. Given $\rho(r_i)$, Eq.(1) determines also the initial velocity at $r = r_i$ for each \dot{M} .

We here explore the effects of the assumed boundary condition and the mass outflow rate \dot{M} on the results of calculated quantities of the neutrino-driven winds. We show in Figs. 1(a) and 1(b) the fluid velocity and the temperature as a function of radius from the center of neutron star for various \dot{M} , where neutron star mass $M = 1.4 M_\odot$ and neutrino luminosity $L_{\nu_e} = 10^{51} \text{ ergs/s}$ are used. Figures 2(a) and 2(b) are the same as those in Figs. 1(a) and 1(b) for $M = 2.0 M_\odot$ and $L_{\nu_e} = 10^{52} \text{ ergs/s}$. Varied \dot{M} 's are tabulated in Table 1 with the calculated entropies and dynamic timescales. These figures indicate that both velocity and temperature profiles are very sensitive to the adopted \dot{M} corresponding to different boundary conditions at $r = 10000 \text{ km}$. However, the entropies are more or less similar to one another, while exhibiting very different dynamic timescales.

Although finding an appropriate boundary condition is not easy, it is one of preferable manners to match the condition obtained in numerical simulations of the supernova explosion. We studied one of the successful simulations of $20M_\odot$ supernova explosion assuming $M = 1.4M_\odot$ (Wilson 1998). Extensive studies of the r-process (Woosley et al. 1994) are based on his supernova model. Careful observation tells us that, although the neutrino luminosity for each flavor changes from $5 \times 10^{52} \text{ ergs/s}$ to 10^{50} ergs/s , the temperature lowers progressively to 0.1 MeV around $r = 10,000 \text{ km}$ where the shock front almost stays during ~ 10 s after the core bounce at times which we are most interested in. It is to be noted that for successful r-process (Woosley et al. 1994) the temperature has to decrease gradually down to around 0.1 MeV at the external region. This will be discussed in later sections. As displayed in Figs.

1(a) and 1(b), our calculation denoted by "3" meets with this imposed boundary condition. Although it may not be necessarily clear, we can adopt the same boundary condition for different neutron star masses which we study in this article, expecting that the physics continuously changes and also aiming at comparing the results with one another which arise from the same boundary condition. Even in the case of massive neutron star having $M = 2.0M_\odot$, as displayed in Figs. 2(a) and 2(b), we can still find a solution denoted by "1" which satisfies the same outer boundary condition. Although we fortunately found a solution with reasonable value of \dot{M} , careful studies of the numerical simulation in the case of massive neutron stars are highly desirable in order to find better boundary condition.

Let us discuss how our adopted outer boundary condition is not unreasonable. We are interested in the times $1s \lesssim t$ when the neutrino-driven wind becomes quasi steady state flow between the neutrinosphere and the shock front. Intense flux of neutrinos from the hot proto-neutron star have already interacted efficiently with radiation and relativistic electron-positron pairs at high temperature. Thus we have $T \sim T_\nu$, where T and T_ν are respectively the photon and neutrino temperatures. In this stage, the gain radius R_g (Bethe & Wilson 1985) at which the neutrino heating and cooling balance with each other is very close to the neutrinosphere. Since we make an approximation that the neutrinosphere and the neutron star surface is close enough, we here assume that the gain radius is also the same, i.e. $R_g = R_\nu = R$. On these conditions we can estimate the mass outflow rate \dot{M} by considering the energy deposition to the gas from the main processes of neutrino capture on nucleons (6) and (7).

Following the discussion by Woosley et al. (1994), the rate of energy deposition in the gas above the neutrinosphere is given by

$$\dot{E} = (L_{\nu_e} + L_{\bar{\nu}_e}) \times \tau_\nu, \quad (17)$$

where τ_ν is the optical depth for the processes (6) and (7) and is given in terms of the opacity κ_ν and the pressure scale height L_p by,

$$\begin{aligned} \tau_\nu &= \int_\infty^{R_g} \kappa_\nu \rho_b dr \\ &\approx \kappa_\nu(R_g) \rho_b(R_g) L_p(R_g) \\ &\approx 0.076 R_7^2 \left(\frac{T_\nu}{3.5 \text{ MeV}} \right)^6 \left(\frac{1.4 M_\odot}{M} \right). \end{aligned} \quad (18)$$

Note that $R_g = R$ and $T_\nu = T_i$. In order to obtain this expression, we have already used an approximate opacity (Bethe 1990, Woosley & Weaver 1993) $\kappa_\nu \approx 6.9 \times 10^{-18} (T_\nu/3.5 \text{ MeV})^2 \text{ cm}^2 \text{ g}^{-1}$ and the pressure scale height in radiation dominated domain which is written as,

$$\begin{aligned} L_p &\approx (aT^4)/(GM\rho_b/R^2) \\ &= 74 \text{ km} \left(\left(\frac{T}{\text{MeV}} \right)^4 R_7^2 / \rho_{b,7} \right) \left(\frac{1.4 M_\odot}{M} \right), \end{aligned} \quad (19)$$

where the subscripts on R_7 and $\rho_{b,7}$ indicate cgs multipliers in units of 10^7 . The energy deposition Eq.(17) is mostly used for lifting the matter out of the gravitational well of the neutron star. Thus, inserting Eq.(18) into Eq.(17) and using the relation $L_{\nu_e} = L_{\bar{\nu}_e} = (7/4)\pi R^2 \sigma T_\nu^4$, the mass outflow rate \dot{M} is approximately given by

$$\begin{aligned} \dot{M} &\approx \dot{E}/(GM/R) \\ &\approx 0.092 \left(\frac{L_{\nu_e} + L_{\bar{\nu}_e}}{10^{53} \text{ ergs s}^{-1}} \right)^{5/2} \left(\frac{1.4 M_\odot}{M} \right)^2 M_\odot \text{ s}^{-1}. \end{aligned} \quad (20)$$

Our mass outflow rate \dot{M} obtained from the imposed boundary condition of a temperature 0.1 MeV at 10,000 km is in reasonable agreement with the estimate using this Eq. (20) within a factor of five for $10^{50} \text{ ergs/s} \leq (L_{\nu_e} + L_{\bar{\nu}_e}) \leq 10^{52} \text{ ergs/s}$.

2.3. Characteristics of the neutrino-driven wind

When the material of the wind is on the surface of the neutron star and neutrinosphere, thermodynamic quantities still reflect the effects of neutralization and the electron fraction Y_e remains as low as ~ 0.1 . Once the wind leaves surface after the core bounce, electron number density decreases abruptly and the chemical equilibrium among leptons is determined by the balance between the two processes (6) and (7) due to intense neutrino fluxes, shifting Y_e to ~ 0.5 . Interesting phase starts when the temperature falls to $\sim 10^{10}$ K, for our purpose of studying the physical condition of the neutrino-driven wind that is suitable for the r-process nucleosynthesis. At this temperature the material is still in the NSE, and the baryon numbers are carried by only free protons and neutrons. The neutron-to-proton number abundance ratio is determined by Y_e for charge neutrality.

Electron antineutrino has a harder spectrum than electron neutrino, as evident from their energy moments $\epsilon_{\nu_e} = 12 \text{ MeV} < \epsilon_{\bar{\nu}_e} = 22 \text{ MeV}$. Thus, the material is slightly shifted to neutron-rich. Assuming weak equilibrium, this situation is approximately described by

$$Y_e \approx \frac{\lambda_{\nu_e n}}{\lambda_{\nu_e n} + \lambda_{\bar{\nu}_e p}} \approx \left(1 + \frac{L_{\bar{\nu}_e} \epsilon_{\bar{\nu}_e} - 2\delta + 1.2\delta^2/\epsilon_{\bar{\nu}_e}}{L_{\nu_e} \epsilon_{\nu_e} + 2\delta + 1.2\delta^2/\epsilon_{\nu_e}} \right)^{-1}, \quad (21)$$

where $\lambda_{\nu_e n}$ and $\lambda_{\bar{\nu}_e p}$ are the reaction rates for the processes (6) and (7), respectively, and δ is the neutron-proton mass difference (Qian & Woosley 1996). In our parameter set of the neutron star mass $M = 1.4M_\odot$ and radius $R = 10 \text{ km}$, for example, Y_e varies from $Y_e(r = R) = 0.43$ to $Y_e(r = 10000\text{km}) = 0.46$ very slowly due to the redshift factor (10) because of $\epsilon \propto \Phi$. As this change is small and the calculated result of hydrodynamic quantities are insensitive to Y_e , we set $Y_e = 0.5$ for numerical simplicity.

One of the most important hydrodynamic quantity, that characterizes the expansion dynamics of the neutrino-driven wind, is the dynamic time scale τ_{dyn} which is the duration time of the α -process. When the temperature falls below 10^{10} K , the NSE favors a composition of alpha-particles and neutrons. As the temperature drops further below about $5 \times 10^9 \text{ K}$ ($T \approx 0.5 \text{ MeV}$), the system falls out of the NSE and the α -process starts accumulating some amount of seed elements until the charged particle reactions freeze out at $T \approx 0.5/e \text{ MeV} \approx 0.2 \text{ MeV}$. Introducing a time variable of the wind moving away from the distance r_i to outer distance r_f

$$\tau = \int_{r_i}^{r_f} \frac{dr}{u}, \quad (22)$$

and setting $r_i = r(T = 0.5\text{MeV})$ and $r_f = r(T = 0.5/e \text{ MeV})$, we can define the dynamic time scale τ_{dyn} by

$$\tau_{\text{dyn}} \equiv \int_{T=0.5\text{MeV}}^{T=0.5/e \text{ MeV}} \frac{dr}{u}. \quad (23)$$

The second important hydrodynamic quantity, that affects strongly the r-process nucleosynthesis which occurs at later times when the temperature cools below 0.2 MeV , is the entropy per baryon, defined by

$$S = \int_R^r \frac{m_N \dot{q}}{uT} dr, \quad (24)$$

where \dot{q} is the total net heating rate (16). As $S \propto T^3/\rho_b$ assuming the radiation dominance, high entropy and high temperature characterizes a system with many photons and low baryon number density. Since high entropy favors also a large fraction of free nucleons in the limit of the NSE, it is expected to be an ideal condition for making high neutron-to-seed abundance ratio. Therefore, the high entropy at the beginning of the α -process is presumed to be desirable for successful r-process.

3. Numerical results

3.1. Effects of relativistic gravity to entropy

The purpose of this section is to discuss both similarities and differences of the neutrino-driven wind between the relativistic treatment and the Newtonian treatment. In Fig. 3, we show typical numerical results of radial velocity u , temperature T , and baryon mass density ρ_b of the wind for the neutron star mass $M = 1.4M_\odot$, radius $R = 10\text{km}$, and the neutrino luminosity $L_\nu = 10^{51} \text{ ergs/s}$. The radial dependence of these quantities is displayed by solid and dashed curves for Schwarzschild and Newtonian cases, respectively, in this figure. Using these results and Eq.(24), we can calculate S in each ejecta. Figure 4 shows the calculated profile of the entropy S for the two cases. Although both entropies describe rapid increase just above the surface of the neutron star $10 \text{ km} \leq r \leq 15 \text{ km}$, the asymptotic value in general relativistic wind is nearly 40 % larger than that in Newtonian wind.

The similar behavior of rapid increase in both winds is due to efficient neutrino heating near the surface of the neutron star. We show the radial dependence of the heating and cooling rates by neutrinos in Figs. 5(a)-(c). Figure 5(a) shows the total net heating rate defined by Eq. (16), and Figs. 5(b) and (c) display the decompositions into contribution from each heating(solid) or cooling(dashed) rate in Schwarzschild and Newtonian cases, respectively. The common characteristic in both cases is that net heating rate \dot{q} has a peak around $r \approx 12 \text{ km}$, which makes a rapid increase in S near the surface of the neutron star for the following reason. The integrand of the entropy S in Eq. (24) consists of the heating rate and the inverse of fluid velocity times temperature. The fluid velocity increases more rapidly than the slower decrease in the temperature, as shown in Fig. 3, after the wind lifts off the surface of the neutron star.

Let us carefully discuss the reason why the general

relativistic wind results in 40 % larger entropy than the Newtonian wind in the asymptotic region. This fact has been suggested in the previous papers of Qian & Woosley (1996) and Cardall & Fuller (1997). Unfortunately, however, the reason of this difference was not clearly appreciated to the specific effect quantitatively among several possible sources.

We first consider the redshift effect and the bending effect of the neutrino trajectory. The redshift effect plays a role in decreasing the mean neutrino energy ϵ_ν ejected from the neutrinosphere, and in practice ϵ_ν is proportional to the redshift factor $\Phi(r)$ which is defined by Eq. (10). Since neutrino luminosity is proportional to Φ^4 and the heating rate \dot{q}_1, \dot{q}_3 , and \dot{q}_5 depend on these quantities in different manners, each heating rate has different Φ -dependence as $\dot{q}_1 \propto L_\nu \epsilon_\nu^2 \propto \Phi^6$, $\dot{q}_3 \propto L_\nu \epsilon_\nu \propto \Phi^5$, and $\dot{q}_5 \propto L_\nu^2 \epsilon_\nu \propto \Phi^9$, as shown in Eqs. (8), (11), and (12). Cooling rates \dot{q}_2 and \dot{q}_4 do not depend on $\Phi(r)$. The bending effect of the neutrino trajectory is included in the geometrical factors $g_1(r)$ and $g_2(r)$ in these equations. Although numerical calculations were carried out by including all five heating and cooling processes, as \dot{q}_1, \dot{q}_2 , and \dot{q}_3 predominate the total net heating rate \dot{q} , we here discuss only these three processes in the following discussions for simplicity.

In Newtonian analysis, the redshift factor $\Phi(r)$ is unity and the geometrical factor is given by

$$g_{1N}(r) = \sqrt{1 - \left(\frac{R_\nu}{r}\right)^2}.$$

This geometrical factor $g_1(r)$ and the redshift factor appear in the form of $(1 - g_1(r))\Phi(r)^m$ in the heating rate \dot{q}_1 ($m = 5$) and \dot{q}_3 ($m = 6$). As for the first factor $(1 - g_1(r))$, the following inequality relation holds between the Schwarzschild and Newtonian cases, for $R_\nu \leq r$;

$$(1 - g_1(r)) > (1 - g_{1N}(r)).$$

However, $\Phi(r)$ is a monotonously decreasing function of r , the combined factor $(1 - g_1(r))\Phi(r)^m / (1 - g_{1N}(r))$ increases from unity and has a local maximum around $r \sim R_\nu + 0.2$ km. Its departure from unity is at most 3 %. Beyond this radius the function starts decreasing rapidly because of the redshift effect $\Phi(r)^m$, and it becomes as low as ~ 0.6 at $r \sim 30$ km. In this region, the net heating rate in the relativistic wind is smaller than that in the Newtonian wind if the temperature and density are the same. However, the

difference in this region does not influence the dynamics of the wind very much. It is almost determined in the inner region $R_\nu \leq r \lesssim 15$ km where one finds efficient neutrino heating and small difference between $(1 - g_1(r))\Phi^m(r)$ and $(1 - g_{1N}(r))$.

By performing general relativistic calculation and neglecting these two relativistic effects, *i.e.* the redshift effect and the bending effect of the neutrino trajectory, we find that it produces only a small change in entropy by $\Delta S \sim 3$. Thus it does not seem to be the major source of the increase in the entropy.

Let us consider another source of general relativistic effects which are included in the solution of a set of the basic equations (1)-(3). Since the entropy depends on three hydrodynamic quantities $\dot{q}(r)$, $u(r)$, and $T(r)$ (see Eq.(24)), we should discuss each quantity. The neutrino-heating rate, $\dot{q}(r)$, depends on the temperature $T(r)$ and density $\rho_b(r)$ in addition to the redshift factor and the geometrical factor of the bending neutrino trajectory. Therefore, we study first the detailed behavior of $T(r)$, $u(r)$, and $\rho_b(r)$, and then try to look for the reason why the general relativistic effects increase the entropy. We assume that the pressure and internal energy per baryon are approximately described by the radiation and relativistic electrons and positrons in order to make clear the following discussions. This is a good approximation for the neutrino-driven wind. The equations of state are given by

$$P \approx \frac{11\pi^2}{180} T^4, \quad (25)$$

$$\epsilon \approx \frac{11\pi^2}{60} \frac{T^4}{\rho_b}. \quad (26)$$

By using another approximation

$$u^2 \ll \frac{4P}{3\rho_b}, \quad (27)$$

which is satisfied in the region of interest, we find

$$\begin{aligned} \frac{1}{T} \frac{dT}{dr} &\approx \frac{1}{1 + u^2 - \frac{2M}{r}} \frac{\rho_b + P}{4P} \\ &\times \left(-\frac{M}{r^2} + \frac{2u^2}{r} - \frac{45}{11\pi^2} \frac{u\rho_b}{T^4} \dot{q} \right), \end{aligned} \quad (28)$$

in Schwarzschild case. The basic equations of the spherically symmetric and steady state wind in Newtonian case are given by

$$\dot{M} = 4\pi r^2 \rho_b v, \quad (29)$$

$$v \frac{dv}{dr} = -\frac{1}{\rho_b} \frac{dP}{dr} - \frac{M}{r^2}, \quad (30)$$

$$\dot{q} = v \left(\frac{d\epsilon}{dr} - \frac{P}{\rho_b^2} \frac{d\rho_b}{dr} \right), \quad (31)$$

where v is the fluid velocity. The equations of state are given by Eqs. (4) and (5) the same as in Schwarzschild case. Repeating the same mathematical technique in Eqs. (29)-(31) instead of Eqs. (1)-(3) and taking the same approximations as (25)-(27), we find the equation corresponding to Eq. (28), in Newtonian case, as

$$\frac{1}{T} \frac{dT}{dr} \approx \frac{\rho_b}{4P} \left(-\frac{M}{r^2} + \frac{2v^2}{r} - \frac{45}{11\pi^2} \frac{v\rho_b}{T^4} \dot{q} \right). \quad (32)$$

Note that the logarithmic derivative of the temperature, $d \ln T / dr = T^{-1} dT / dr$, has always a negative value, and the temperature is a monotonously decreasing function of r . There are two differences between Eqs. (28) and (32). The first prefactor $1/(1 + u^2 - 2M/r)$ in the r.h.s. of Eq. (28) is larger than unity. This causes more rapid decrease of $T(r)$ in relativistic case than in Newtonian case at small radii within $r \sim 20$ km, as shown in Fig. 3, where our approximations are satisfied. The second prefactor $(\rho_b + P)/4P$ in the r.h.s. of Eq. (28) is larger than the prefactor $\rho_b/4P$ in the r.h.s. of Eq. (32), *i.e.* $(\rho_b + P)/4P > \rho_b/4P$, which also makes the difference caused by the first prefactor even larger.

Applying the similar mathematical transformations to the velocity, we obtain the following approximations,

$$\frac{1}{u} \frac{du}{dr} \approx \frac{3}{1 + u^2 - \frac{2M}{r}} \frac{(\rho_b + 4P)}{4P} \frac{M}{r^2} - \frac{2}{3r} + \frac{\rho_b}{4uP} \dot{q} \quad (33)$$

in Schwarzschild case, and

$$\frac{1}{v} \frac{dv}{dr} \approx \frac{3\rho_b}{4P} \frac{M}{r^2} - \frac{2}{3r} + \frac{\rho_b}{4vP} \dot{q} \quad (34)$$

in Newtonian case. In these two equations, the first leading term in the r.h.s. makes the major contribution. Since exactly the same prefactors $1/(1 + u^2 - 2M/r)$ and $(\rho_b + 4P)/4P$ appear in Schwarzschild case, the same logic as in the logarithmic derivative of the temperature is applied to the velocity. Note, however, that slightly different initial velocities at the surface of the neutron star make this difference unclear in Fig. 3. The relativistic Schwarzschild wind starts from $u(10 \text{ km}) \approx 8.1 \times 10^4 \text{ cm/s}$, while the Newtonian wind starts from $v(10 \text{ km}) \approx 2.0 \times 10^5 \text{ cm/s}$. Both

winds reach almost the same velocity around $r \sim 20$ km or beyond.

The baryon number conservation leads to the logarithmic derivative of the baryon density

$$\frac{1}{\rho_b} \frac{d\rho_b}{dr} = -\frac{1}{u} \frac{du}{dr} - \frac{2}{r}, \quad (35)$$

where u is the radial component of the four-velocity in Schwarzschild case. The fluid velocity v should read for u in Newtonian case. Inserting Eq. (33) or Eq. (34) to the first leading term of the r.h.s. of this equation, we can predict the behavior of ρ_b as a function of r in both Schwarzschild and Newtonian cases as shown in Fig. 3.

Incorporating these findings concerning $T(r)$, and $u(r)$ into the definition of entropy Eq. (24), we can now discuss why the relativistic Schwarzschild wind makes larger entropy than the Newtonian wind. We have already discussed previously in the second paragraph of this section that the fluid velocity increases more rapidly in Schwarzschild case. Since integrand of the entropy S is inversely proportional to fluid velocity times temperature, this fact enlarges the difference due to \dot{q} at smaller radii (see Fig. 4(a)). In addition, as we found, temperature in Schwarzschild geometry is smaller than the temperature in Newtonian geometry. For these reasons, the entropy in the relativistic Schwarzschild wind becomes larger than the entropy of the Newtonian wind.

Let us confirm the present results quantitatively in a different manner. The entropy per baryon for relativistic particles with zero chemical potential is given by

$$S = \frac{11\pi^2}{45} \frac{T^3}{\rho_b/m_N}. \quad (36)$$

Here, we take a common temperature $T = 0.5 \text{ MeV}$ to each other in Schwarzschild and Newtonian cases. This is the typical temperature at the beginning of the α -process, and both electrons and positrons are still relativistic at this temperature. We read off the radii at which the temperature becomes 0.5 MeV in Fig. 3. They are 43 km and 55 km in Schwarzschild and Newtonian cases, respectively. We can again read off the baryon mass densities at these radii in this figure, that are $\rho_b = 5.5 \times 10^5 \text{ g/cm}^3$ at $r = 43 \text{ km}$ in relativistic Schwarzschild wind and $\rho_b = 7.8 \times 10^5 \text{ g/cm}^3$ at $r = 55 \text{ km}$ in Newtonian wind. Taking the inverse ratio of these ρ_b values with approximate relation (36), we find that the entropy in Schwarzschild

case is 40 % larger than that in Newtonian case. This is quantitatively in good agreement with the result of numerical calculation shown in Fig. 4.

Let us shortly remark on the dynamic time scale τ_{dyn} . Although higher entropy is favorable for making enough neutrons in the neutrino-driven wind, shorter dynamic time scale also is in favor of the r-process. This is because the neutron-to-seed abundance ratio, which is one of the critical parameters for successful r-process, becomes larger in the wind with shorter τ_{dyn} , which is to be discussed in the next section. It is therefore worth while discussing the general relativistic effect on τ_{dyn} here. The argument is very transparent by using Eqs. (28) and (32) and Fig. 3. Since the dynamic time scale τ_{dyn} is defined as the duration of α -process in which the temperature of the wind cools from $T = 0.5$ MeV to $T = 0.5/e \approx 0.2$ MeV, faster cooling is likely to result in shorter τ_{dyn} . Let us demonstrate it numerically. For the reasons discussed below two Eqs. (28) and (32), the relativistic fluid describes more rapid decrease in temperature than the Newtonian fluid as a function of distance r . In fact, the distance corresponding to $T = 0.5 - 0.2$ MeV are $r = 43 - 192$ km in Schwarzschild case, and $r = 55 - 250$ km in Newtonian case. Figure 3 tells us that both fluids have almost the same velocities at these distances, which gives shorter τ_{dyn} for the Schwarzschild case than the Newtonian case. The calculated dynamic time scales are $\tau_{\text{dyn}} = 0.164$ s for the former and $\tau_{\text{dyn}} = 0.213$ s for the latter.

Before closing this subsection, let us briefly discuss how the system makes a complicated response to the change in $T(r)$, $u(r)$ and $\rho_b(r)$. When the temperature decreases rapidly at $10 \text{ km} \lesssim r \lesssim 20 \text{ km}$, the major cooling process of the e^+e^- capture by free nucleons, \dot{q}_2 , is suppressed because this cooling rate has rather strong temperature dependence, $\dot{q}_2 \propto T^6$. In Schwarzschild geometry this suppression partially offsets the decrease in \dot{q}_1 due to the neutrino redshift effect, though being independent of temperature of the wind. Another heating source \dot{q}_3 due to neutrino-electron scattering also plays a role in the change of entropy. Since \dot{q}_3 depends on the baryon density as well as temperature $\dot{q}_3 \propto T^4/\rho_b$, if the system has a correlated response to decrease ρ_b strongly with decreasing temperature, then this might eventually work for the partial increase in entropy. However, in reality, actual response arises from more complicated mechanism because \dot{q}_i 's should depend on the solution of dynamic equations (1)-(3) self-consistently on

adopted proper boundary conditions and input parameters through the relation $\dot{q}_1 \propto L_\nu \epsilon_\nu^2$, $\dot{q}_2 \propto T^6$, $\dot{q}_3 \propto T^4/\rho_b L_\nu \epsilon_\nu$, $\dot{q}_4 \propto T^9/\rho_b$, and $\dot{q}_5 \propto \rho_b^{-1} L_\nu^2 \epsilon_\nu$. The neutrino-driven wind is a highly non-linear system.

3.2. Parameter dependence

Most of the previous studies of the neutrino-driven wind have been concentrated on SN1987A, and the parameter set in the theoretical calculations was almost exclusive. We here expand our parameter region of the neutron star mass M , radius R , and neutrino luminosity L_ν , and investigate widely the dependence of key quantities, τ_{dyn} and S , on these three parameters. Since the neutron star mass M and radius R are mostly contained through the form M/R in the basic equations of the system, we only look at the dependence on M and L_ν .

Figures 6(a) and 6(b) show the calculated τ_{dyn} and S at the beginning of the α -process at $T = 0.5$ MeV for various neutron star masses $1.2M_\odot \leq M \leq 2.0M_\odot$. Closed circles, connected by thick solid line, and open triangles, connected by thin solid line, are those for the Schwarzschild and Newtonian cases. In Fig. 6(a), we plot also two broken lines in Newtonian case from the paper (Qian and Woosley 1996) which adopted

$$\tau_{\text{dyn}}(\text{QW}) = \left. \frac{r}{v} \right|_{0.5 \text{ MeV}}, \quad (37)$$

in two limits of the radiation dominance (upper) and the dominance of non-relativistic nucleon (lower). In either limit, this $\tau_{\text{dyn}}(\text{QW})$ is an increasing function of the neutron star mass and this feature is in reasonable agreement with our exact solution Eq.(23). However, absolute value of (37) is about half that of the exact solution in the Newtonian case.

Remarkable difference between Schwarzschild and Newtonian cases is an opposite response of τ_{dyn} to the neutron star mass (Fig. 6(a)). General relativistic effects make the dynamic time scale even smaller with increasing neutron star mass. We have already discussed the reason why τ_{dyn} in Schwarzschild case is smaller than that in Newtonian case by comparing Eqs. (28) and (32) from each other. We understand the decrease of τ_{dyn} as a consequence from the fact that the general relativistic effects, which arise from the two prefactors in the r.h.s. of Eq.(28), are enlarged by stronger gravitational force M/r^2 with larger M . Similar analysis on the role of the gravitational force is applied to the discussion of entropy and

Eqs. (28), (33), and (35). Figure 6(b) displays that the entropy per baryon in Schwarzschild case makes stronger mass dependence than in Newtonian case.

It is to be noted again that the above features of the mass dependence are equivalent to those obtained by the change in the neutron star radius. Since the radius of protoneutron star shrinks with time in cooling process, it may work for increasing the entropy and decreasing the dynamic time scale.

Figures 7(a) and 7(b) show the dependence of our calculated τ_{dyn} and S on the neutrino luminosity ranging $10^{50} \text{ ergs/s} \leq L_\nu \leq 10^{52} \text{ ergs/s}$. Differing from the mass dependence, both quantities are decreasing function of L_ν as far as $L_\nu \leq 10^{52} \text{ ergs/s}$. This tendency, except for the absolute values, is in reasonable agreement with approximate estimates (Qian and Woosley 1996) shown by broken lines. This is because larger luminosity makes the mass outflow rate \dot{M} higher through more efficient neutrino heating, which causes bigger increase in the fluid velocity in addition to moderate increase in baryon density. Having these changes in hydrodynamic quantities with the definition of τ_{dyn} , Eq.(23), and the definition of S , Eq.(24), we understand that both quantities decrease with increasing neutrino luminosity.

However, if the luminosity becomes larger than 10^{52} ergs/s , the temperature does not decrease as low as 0.1 MeV before the distance reaches 10000 km because of the effect of too strong neutrino heating. The dynamic time scale τ_{dyn} is of order $\sim 10 \text{ s}$. In such a very slow expansion of the neutrino-driven wind, α -process goes on and leads to uninteresting r-process nucleosynthesis.

To summarize this section, we find it difficult to obtain very large entropy ~ 400 for reasonably short dynamic time scale $\tau_{\text{dyn}} \lesssim 0.1 \text{ s}$, as reported by Woosley et al. (1994), by changing the neutron star mass M and neutrino luminosity L_ν . However, there are still significant differences between our calculated result of τ_{dyn} and S , which are shown by thick solid lines in Figs. 6(a)-7(b), and those of Qian and Woosley (1996), which are shown by broken lines, in the mass dependence of the entropy and the opposite behavior in τ_{dyn} . We will see in the subsequent sections that these differences are important to look for successful condition of the r-process.

3.3. Implication in nucleosynthesis

Having known the detailed behavior of dynamic time scale τ_{dyn} and entropy per baryon S as a function of neutron star mass M , radius R , and neutrino luminosity L_ν , we are forced to discuss their implication in the r-process nucleosynthesis. We have already shown the calculated results of τ_{dyn} and S for limited sets of two independent parameters M and L_ν in Figs. 6(a)-7(b). We here expand the parameter space in order to include a number of (M, L_ν) -grids in their reasonable range $1.2M_\odot \leq M \leq 2.0M_\odot$ and $10^{50} \text{ ergs/s} \leq L_\nu \leq 10^{52} \text{ ergs/s}$.

Figure 8 displays the calculated results in the $\tau_{\text{dyn}} - S$ plane. Shown also are two zones for which the r-process nucleosynthesis might occur so that the second abundance peak around $A = 130$ and the third abundance peak around $A = 195$ emerge from a theoretical calculation as suggested by Hoffman et al. (1997). Their condition for the element with mass number A to be produced in an explosive r-process nucleosynthesis, for $Y_e > \langle Z \rangle / \langle A \rangle$, is given by

$$S \approx Y_{e,i} \left\{ \frac{8 \times 10^7 (\langle A \rangle - 2\langle Z \rangle)}{\ln[(1 - 2\langle Z \rangle / A) / (1 - \langle A \rangle / A)]} \left(\frac{\tau_{\text{dyn}}}{\text{sec}} \right) \right\}^{1/3}, \quad (38)$$

where $\langle A \rangle$ is mean mass number and $\langle Z \rangle$ is mean proton number of the seed nuclei at the end of the α -process. Following numerical survey of seed abundance of Hoffman et al. (1997), we choose $\langle A \rangle = 90$ and $\langle Z \rangle = 34$ in Fig. 8. From this figure, we find that dynamic time scale as short as $\tau_{\text{dyn}} \approx 6 \text{ ms}$ with $M = 2.0M_\odot$ and $L_\nu = 10^{52} \text{ ergs/s}$ is the best case among those studied in the present paper in order to produce the r-process elements, although the entropy S is rather small 140.

Let us remark shortly on this useful equation. Equation (38) tells us that the r-process element with mass number A is efficiently produced from seed elements with $\langle A \rangle$ and $\langle Z \rangle$ on a given physical condition τ_{dyn} , S , and Y_e at the onset of r-process nucleosynthesis at $T_9 \approx 2.5$. In order to derive Eq. (38), Hoffman et al. (1997) assumed that the $\alpha + \alpha + n \rightarrow {}^9\text{Be} + \gamma$ reaction is in equilibrium, because of its low Q-value, during the α -process at $T \approx 0.5 - 0.2 \text{ MeV}$ and that the ${}^9\text{Be} + \alpha \rightarrow {}^{12}\text{C} + \gamma$ reaction triggers burning of alpha-particles to accumulate seed elements. The NSE holds true if the nuclear interaction time scale for $\alpha + \alpha + n \rightarrow {}^9\text{Be} + \gamma$ is much shorter than the expansion time scale. We found in the present calculation that it is not always the case in neutrino-driven winds

with short dynamic time scale, for $L_\nu \approx 5 \times 10^{51} - 10^{52}$ ergs/s, which is to be discussed more quantitatively in the next section. Keeping this in mind, we think that Eq. (38) is still a useful formula in order to search for suitable physical condition for the r-process without performing numerical nucleosynthesis calculation.

One might wonder if the dynamic time scale $\tau_{\text{dyn}} \sim 6$ ms is too short for the wind to be heated by neutrinos. Careful comparison between proper expansion time and specific collision time for the neutrino heating is needed in order to answer this question. Note that τ_{dyn} was defined as the duration of the α -process so that the temperature of the expanding wind decreases from $T = 0.5$ MeV to $0.5/e \approx 0.2$ MeV, which correspond to outer atmosphere of the neutron star. These radii are $r(T = 0.5 \text{ MeV}) = 52$ km and $r(T = 0.5/e \text{ MeV}) = 101$ km for the wind with $(L_\nu, M) = (10^{52} \text{ ergs/s}, 2.0 M_\odot)$, and $r(T = 0.5 \text{ MeV}) = 43$ km and $r(T = 0.5/e \text{ MeV}) = 192$ km for the wind with $(L_\nu, M) = (10^{51} \text{ erg/s}, 1.4 M_\odot)$. We found in Figs. 5(a)-(c) that the neutrinos transfer their kinetic energy to the wind most effectively just above the neutron star surface at $10 \text{ km} \leq r < 20 \text{ km}$. Therefore, as for the heating problem, one should refer the duration of time for the wind to reach the radius where temperature is $T \approx 0.5$ MeV rather than τ_{dyn} . We can estimate this expansion time τ_{heat} by setting $r_i = R = 10$ km and $r_f = r(T = 0.5 \text{ MeV})$ in Eq. (22): $\tau_{\text{heat}} = 0.017$ s and 0.28 s for the winds with $(L_\nu, M) = (10^{52} \text{ ergs/s}, 2.0 M_\odot)$ and $(10^{51} \text{ ergs/s}, 1.4 M_\odot)$, respectively. We note, for completeness, $r(T = 0.5 \text{ MeV}) = 52$ km or 43 km for each case.

These proper expansion time scales, τ_{heat} , are to be compared with the specific collision time τ_ν for the neutrino-nucleus interactions in order to discuss the efficiency of the neutrino heating. The collision time τ_ν is expressed (Qian et al. 1997) as

$$\tau_\nu \approx 0.201 \times L_{\nu,51}^{-1} \times \left(\frac{\epsilon_\nu}{\text{MeV}} \right) \left(\frac{r}{100 \text{ km}} \right)^2 \left(\frac{\langle \sigma_\nu \rangle}{10^{-41} \text{ cm}^2} \right)^{-1} \quad (39)$$

where $L_{\nu,51}$ and ϵ_ν have already been defined in Sec. 2-1, and $\langle \sigma_\nu \rangle$ is the averaged cross section over neutrino energy spectrum. As discussed above, neutrino heating occurs most effectively at $r \approx 12$ km (see also Fig. 5(a)), and we set this value in Eq. (39). Since two neutrino processes (6) and (7) make the biggest contribution to heating the wind and $\epsilon_{\bar{\nu}_e} = 12$

MeV and $\epsilon_{\bar{\nu}_e} = 22$ MeV, we set $\epsilon_\nu = (\epsilon_{\nu_e} + \epsilon_{\bar{\nu}_e})/2 \approx 15$ MeV. We take $\langle \sigma_\nu \rangle = 10^{-41} \text{ cm}^2$. Incorporating these values into Eq. (39), we can obtain τ_ν value. Let us compare the specific collision time, τ_ν , and the proper expansion time, τ_{heat} , with each other:

$$\begin{aligned} \tau_\nu &= 0.0043 \text{ s} < \tau_{\text{heat}} = 0.017 \text{ s}, \\ &\text{for } (L_\nu, M) = (10^{52} \text{ ergs/s}, 2.0 M_\odot), \end{aligned} \quad (40a)$$

$$\begin{aligned} \tau_\nu &= 0.043 \text{ s} < \tau_{\text{heat}} = 0.28 \text{ s}, \\ &\text{for } (L_\nu, M) = (10^{51} \text{ ergs/s}, 1.4 M_\odot). \end{aligned} \quad (40b)$$

We can conclude that there is enough time for the expanding wind to be heated by neutrinos even with short dynamic time scale for the α -process, $\tau_{\text{dyn}} \sim 6$ ms, which corresponds to the case (40a).

Before closing this section, let us briefly discuss the effect of electron fraction Y_e on the hydrodynamic condition of the neutrino-driven wind. Although we took $Y_e = 0.5$ for simplicity in our numerical calculations, we should examine the sensitivity of the calculated result on Y_e quantitatively. Since we are interested in short dynamic time scale, let us investigate the case with $(L_\nu, M) = (10^{52} \text{ ergs/s}, 2.0 M_\odot)$ which results in $S = 138.5$ and $\tau_{\text{dyn}} = 0.00618$ s for $Y_e = 0.5$. When we adopt $Y_e = 0.4$, these quantities change slightly to $S = 141.5$ and $\tau_{\text{dyn}} = 0.00652$ sec. These are very small changes less than 5%, and the situation is similar for the other sets of (L_ν, M) .

To summarize this section, we found that there is a parameter region in Fig. 8 which leads to desirable physical condition for the r-process nucleosynthesis. Sophisticated supernova simulation (Woosley et al. 1994) indicates that the neutrino luminosity from the protoneutron star decreases slowly from about 5×10^{52} to 10^{51} ergs/s as the time passes by after the core bounce. Therefore, our favorable neutrino luminosity $L_\nu = 10^{52}$ ergs/s is possible in reality in relatively earlier epoch of supernova explosion at around 0.5 s to a few seconds after the core bounce.

4. R-process nucleosynthesis calculation

Our discussion on the r-process nucleosynthesis in the last section was based on Hoffman's criterion, Eq. (38), which is to be referred with caution for several assumptions and approximations adopted in its derivation. The purpose of this section is to confirm quantitatively that the r-process occurs in the

neutrino-driven wind with short dynamic time scale, which we found in the present study.

Given the flow trajectory characterized by $u(t)$, $\rho_b(t)$, and $T(t)$ as discussed in the last section, our nucleosynthesis calculation starts from the time when the temperature is $T_9 = 9$. Since this temperature is high enough for the system to be in the NSE, initial nuclear composition consists of free neutrons and protons. We set $Y_e = 0.4$ in order to compare with Hoffman's criterion shown in Fig. 8. In our nucleosynthesis calculation we used a fully implicit single network code for the α -process and r-process including over 3000 isotopes. We take the thermonuclear reaction rates for all relevant nuclear processes and their inverse reactions as well as weak interactions from Thielemann (1995) for the isotopes $Z \leq 46$ and from Cowan et al. (1991) for the isotopes $Z > 46$. Previous r-process calculations had complexity that the seed abundance distribution at $T_9 = 2.5$ was not fully shown in literature (Woosley et al. 1994, Woosley & Hoffman 1992, Hoffman, Woosley, & Qian 1997), which makes the interpretation of the whole nucleosynthesis process less transparent. This inconvenience happened because it was numerically too heavy to run both α -process and r-process in a single network code for huge number of reaction couplings among ~ 3000 isotopes. For this reason, one had to calculate the α -process first, using smaller network for light-to-intermediate mass elements, in order to provide seed abundance distribution at $T_9 = 2.5$ ($T \approx 0.2$ MeV). Adopting such seed abundance distribution and following the evolution of material in the wind after $T \approx 0.2$ MeV, which is the onset temperature of the r-process, the r-process nucleosynthesis calculation was extensively carried out by using another network code independent of the α -process. Our nucleosynthesis calculation is completely free from this complexity because we exploited single network code which is applied to a sequence of the whole processes of NSE - α -process - r-process.

The calculated mass abundance distribution is shown in Figs. 10 and 9 for the neutrino-driven wind with $(L_\nu, M) = (10^{52} \text{ ergs/s}, 2.0 M_\odot)$ that makes most favorable condition for the r-process nucleosynthesis with the shortest $\tau_{\text{dyn}} = 0.0062$ s among those studied in the present paper (see Fig. 8). Figure 9 displays the snapshot at the time when the temperature cooled to $T_9 = 2.5$ (≈ 0.2 MeV) at the end of the α -process. This shows seed abundance distribution at the onset of the r-process, too. Our calculated quantities at

this temperature are the baryon mass density $\rho_b = 3.73 \times 10^4 \text{ g/cm}^3$, neutron mass fraction $X_n = 0.159$, mass fraction of alpha-particle $X_\alpha = 0.693$, average mass number of seed nuclei $\langle A \rangle = 94$, and neutron-to-seed abundance ratio $n/s = 99.8$ for the set of hydrodynamic quantities $\tau_{\text{dyn}} = 0.0062$ s, $S \approx 139$, and $Y_e = 0.4$. These values should be compared with those adopted in Woosley's calculation of trajectory 40, *i.e.*, $\rho_b = 1.107 \times 10^4 \text{ g/cm}^3$, $X_n = 0.176$, $X_\alpha = 0.606$, $\langle A \rangle = 95$, $n/s = 77$, $\tau_{\text{dyn}} \approx 0.305$ s, $S \approx 400$, and $Y_e = 0.3835$, as in Table 3 in Woosley et al. (1994). It is interesting to point out that our seed abundance distribution in Fig. 9 is very similar to theirs (Woosley et al. 1994, Woosley & Hoffman 1992), as clearly shown by almost the same $\langle A \rangle \approx 95$, although the other evolutionary parameters and thermodynamic quantities are different from each other. The calculated final r-process abundance is displayed in Fig. 10. Our wind model can produce the second ($A \approx 135$) and third ($A \approx 195$) r-process abundance peaks and rare earth elements between them as well.

It is generally accepted that the r-process elements will be produced if there are plenty of free neutrons and if the neutron-to-seed abundance ratio is high enough to approximately satisfy $A \approx \langle A \rangle + n/s$ (Hoffman, Woosley, & Qian 1997) at the beginning of the r-process, where A is the typical mass number of the r-process element. Therefore, the α -process should take the key to understand why our wind model results in a similar r-process nucleosynthesis to the result of Woosley's trajectory 40.

The α burning starts when the temperature cools below $T = 0.5$ MeV. Since triple alpha reaction ${}^4\text{He}(\alpha\alpha, \gamma){}^{12}\text{C}$ is too slow at this temperature, alternative nuclear reaction path to reach ${}^{12}\text{C}$, ${}^4\text{He}(\alpha n, \gamma){}^9\text{Be}(\alpha, n){}^{12}\text{C}$, triggers explosive α -process to produce the seed elements. In rapidly expanding flow of neutrino-driven wind with short τ_{dyn} , it is not a good approximation to assume that the first reaction ${}^4\text{He}(\alpha n, \gamma){}^9\text{Be}$ is in the NSE. Rate equation is thus written as

$$\begin{aligned} \frac{dY_9}{dt} &\approx \rho_b^2 Y_\alpha^2 Y_n \lambda(\alpha\alpha n \rightarrow {}^9\text{Be}) \\ &- \rho_b Y_\alpha Y_9 \lambda({}^9\text{Be} \alpha \rightarrow {}^{12}\text{C}) \\ &+ (\text{their inverse and} \\ &\quad \text{other reaction rates}), \end{aligned} \quad (41)$$

where Y_9 , Y_α , Y_n are the number fractions of ${}^9\text{Be}$, α , and neutron, and $\lambda(\alpha\alpha n \rightarrow {}^9\text{Be})$ and $\lambda({}^9\text{Be} \alpha \rightarrow {}^{12}\text{C})$ are the thermonuclear reaction rate for each reaction

process as indicated. Details on λ 's are reported in Woosley and Hoffman (1992) and Wrean, Brune, and Kavanagh (1994). Let us take the first term of the *r.h.s.* of Eq. (41) which is largest all terms in Eq. (41). This is allowed in the following discussion of the time scale because the ${}^4\text{He}(\alpha n, \gamma){}^9\text{Be}$ reaction is the slowest among all charged particle reaction paths in all α -process reactions. We now define the typical nuclear reaction time scale τ_α of the α -process, regulated by the ${}^4\text{He}(\alpha n, \gamma){}^9\text{Be}$ reaction time scale τ_N , as

$$\tau_\alpha \gtrsim (\rho_b^2 Y_\alpha^2 Y_n \lambda(\alpha n \rightarrow {}^9\text{Be}))^{-1} \equiv \tau_N. \quad (42)$$

We show the ratio τ_{dyn}/τ_N as a function of the baryon mass density ρ_b at the beginning of the α -process when $T = 0.5$ MeV for various cases of the wind models with (L_ν, M) in Fig. 11. Note that the critical line $\tau_{dyn}/\tau_\alpha = 1$ is slightly shifted upwards because of $\tau_N \lesssim \tau_\alpha$. This figure, with the help of Fig. 8, clearly indicates that the favorable conditions for the r-process nucleosynthesis have inevitably shorter $\tau_{dyn} \ll \tau_N$ and τ_α . Typical ratio is of order $\tau_{dyn}/\tau_N \sim 0.1$. To interpret this result, there is not enough time for the α -process to accumulate a number of seed elements and plenty of free neutrons are left even at the beginning of the r-process. Consequently, the n/s ratio becomes very high ~ 100 .

As for the neutron mass fraction, on the other hand, our value $X_n = 0.159$ is smaller than Woosley's model value $X_n = 0.176$ in trajectory 40 because low entropy is in favor of low neutron fraction. This may be a defect in our low entropy model. However, the short dynamic time scale saves the situation by regulating the excess of the seed elements as discussed above. These two effects compensate with each other to result in average mass number of seed nuclei $\langle A \rangle \approx 95$ and neutron-to-seed abundance ratio $n/s \approx 100$, which is ideal for the production of the third ($A \approx 195$) abundance peak of the r-process elements in our model, as displayed in Fig. 10.

R-process elements have recently been detected in several metal-deficient halo stars (Snedden et al. 1996) and the relative abundance pattern for the elements between the second and the third peak proves to be very similar to that of the solar system r-process abundances. One of the possible and straightforward interpretations of this fact is that they were produced in narrow window of some limited physical condition in massive supernova explosions, as studied in the present paper. These massive stars have short lives $\sim 10^7$ yr and eject nucleosynthesis products into in-

terstellar medium continuously from the early epoch of Galaxy evolution. It is not meaningless, therefore, to discuss several features of our calculated result in comparison with the solar system r-process abundance distribution (Käppeler, Beer, & Wisshak 1989) in Fig. 10. Although Käppeler et al. obtained these abundances as s-process subtractions from the observed meteoritic abundances (Anders and Grevesse 1989) for the mass region $63 \leq A \leq 209$, the inferred yields and error bars for $A = 206, 207, 208$, and 209 are subject to still uncertain s-process contribution. We did not show these heavy elements $A = 206 - 209$ in Fig. 10.

Our single wind model reproduces observed abundance peaks around $A \approx 130$ and $A \approx 195$ and the rare earth element region between these two peaks. However, there are several requirements to the wind model in order to better fit the details of the solar system r-process abundances in the mass region $120 \lesssim A$. The first unsatisfactory feature in our model calculation is that the two peaks are shifted upward by $2 \sim 4$ mass unit, although overall positions and peaks are in good agreement with the solar system data. This is a common problem in all theoretical calculations of the r-process nucleosynthesis (Meyer et al., Woosley et al. 1994). The shift of the peak around $A \approx 195$ is slightly larger than that around $A \approx 130$, which may be attributed to a strong neutron exposure as represented by $n/s \approx 100$ in our model calculation. The second feature is that the rare earth element region shows broad abundance hill, but its peak position $A \approx 165$ in the data is not explained in our calculation. It was pointed out by Surman et al. (1997) that the abundance structure in this mass region is sensitive to a subtle interplay of nuclear deformation and beta decay just prior to the freeze-out of the r-process. More careful studies of these nuclear effects and the dynamics of the r-process nucleosynthesis are desirable. The third failure in the model calculation is the depletion around $A \approx 120$, which is also another serious problem encountered commonly by all previous theoretical calculations. This deficiency is thought to be made by too fast runaway of the neutron-capture reaction flow in this mass region. This is due to too strong shell effects of the $N = 82$ neutron shell closure, suggesting an incomplete nuclear mass extrapolations to the nuclei with $Z \approx 40$ and $N \approx 70 - 80$ which correspond to the depleted abundance mass region $A \approx 120$. It is an interesting suggestion among many others (Woosley et al. 1994) that an artificial

smoothing of extrapolated zigzag structure of nuclear masses could fill the abundance dip around $A \approx 120$. This suggestion sheds light on the improvement of mass formula.

Let us repeat it again that an overall success in the present r-process nucleosynthesis calculation, except for several unsatisfactory fine features mentioned above, is only for heavier mass elements $130 \lesssim A$ including the second ($A \approx 130$) and the third ($A \approx 195$) peaks. When one looks at disagreement of the abundance yields around the first ($A \approx 80$) peak, relative to those at the third peak, between our calculated result and the solar system r-process abundances, it is clear that a single wind model is unable to reproduce all three r-process abundance peaks. The first peak elements should be produced on different conditions with lower neutron-to-seed ratio and higher neutrino flux. It has already been pointed out by several authors (Seeger et al. 1965, Kodama & Takahashi 1975, Hillebrandt, Takahashi, & Kodama 1976) that even the r-process nucleosynthesis needs different neutron exposures similarly to the s-process nucleosynthesis in order to understand the solar system r-process abundance distribution. In a single event of supernova explosion, there are several different hydrodynamic conditions in different mass shells of the neutrino-driven wind (Woosley et al. 1994, Witt, Janka, & Takahashi 1994), which may produce the first peak elements. Different progenitor mass supernova or the event like an exploding accretion disk of neutron-star merger might contribute to the production of the r-process elements. Consideration of these possibilities is beyond our scope in the present paper.

We did not include the effects of neutrino absorption and scattering during the nucleosynthesis process in the present calculation. This is because these effects do not change drastically the final r-process yields as far as the dynamic expansion time scale τ_{dyn} is very short. Using Eq. (39), we can estimate the specific collision time for neutrino-nucleus interaction

$$\tau_\nu \approx 0.082\text{s} - 0.31\text{s}, \quad (43)$$

where the input parameters are set equal to $L_{\nu,51} = 10$, $\epsilon_\nu = 15$ MeV, and $\langle \sigma_\nu \rangle = 10^{-41}$ cm². Note that $\tau_\nu \approx 0.082$ s is the specific neutrino collision time at $r = 52$ km where the temperature of the wind becomes $T = 0.5$ MeV at the beginning of the α -process, and $\tau_\nu \approx 0.31$ s for $r = 101$ km and $T = 0.5/e \approx 0.2$ MeV at the beginning of the r-process. These τ_ν val-

ues are larger than $\tau_{\text{dyn}} = 0.0062$ s that stands for the duration of the α -process by definition. Therefore, the neutrino process does not disturb the hydrodynamic condition of the rapid expansion during the α -process.

It is to be noted, however, that the neutrino process virtually makes the strong effect on the r-process for the winds of slow expansion. We have numerically examined Woosley's model (1994) of trajectory 40 to find $\tau_{\text{dyn}} \approx 0.3$ s. Meyer et al. (1998) also used $\tau_{\text{dyn}} = 0.3$ s in their simplified fluid trajectory to see the neutrino-capture effects. This dynamic time scale $\tau_{\text{dyn}} \approx 0.3$ s is larger than or comparable to the specific neutrino collision time τ_ν in Eq.(43). In such a slow expansion the neutrino absorption by neutron (6) proceeds to make a new proton in the α -process. This proton is quickly interconverted into alpha-particle in the following reaction chain, $p(n, \gamma)d(n, \gamma)t$ which is followed by $t(p, n)^3\text{He}(n, \gamma)^4\text{He}$ and $t(t, 2n)^4\text{He}$, and contributes to the production of seed elements. These radiative capture reactions and nuclear reactions are much faster than the weak process (7) on newly produced proton from the process (6). The net effect of these neutrino processes, therefore, is to decrease the neutron number density and increase the seed abundance, which leads to extremely low n/s ratio. As a result, even the second abundance ($A \approx 130$) peak of the r-process elements disappears, as reported in literature (Meyer, McLaughlin, & Fuller 1998, Meyer 1995). Details on the neutrino process will be reported elsewhere.

We have assumed that electrons and positrons are fully relativistic throughout the nucleosynthesis process. However, the total entropy of the system may change at the temperature $T \lesssim 1/3m_e$ where electrons and positrons tend to behave as non-relativistic particles. This might affect the nucleosynthesis although it does not affect significantly the dynamics near the protoneutron star. We should correct this assumption in the future papers.

Finally, let us refer to massive neutron star. Large dispersion in heavy element abundance of halo stars has recently been observed. Ishimaru and Wanajo (1999) have shown in their galactic chemical evolution model that if r-process nucleosynthesis occurs in either massive supernovae $\geq 30M_\odot$ or small mass supernovae $8 - 10M_\odot$, where these masses are for the progenitors, the observed large dispersion can be well explained theoretically. In addition, SN1994W

and SN1997D are presumed to be due to $25 M_{\odot} - 40 M_{\odot}$ massive progenitors because of very low ^{56}Ni abundance in the ejecta (Sollerman, Cumming, & Lundqvist 1998, Turatto et al. 1998). These massive supernova are known to have massive iron core $\geq 1.8 M_{\odot}$ and leave massive remnant (Turatto et al. 1998). It is critical for the r-process nucleosynthesis whether the remnant is neutron star or black hole. Recent theoretical studies of the EOS of neutron star matter, which is based on relativistic mean field theory, set upper limit of the neutron star mass at $2.2 M_{\odot}$ (Shen et al. 1998).

5. Conclusion and Discussions

We studied the general relativistic effects on neutrino-driven wind which is presumed to be the most promising site for the r-process nucleosynthesis. We assumed the spherically symmetric and steady state flow of the wind. In solving the basic equations for relativistic fluid in Schwarzschild geometry, we did not take approximate method as adopted in several previous studies. We tried to extract generic properties of the wind in manners independent of supernova models or neutron-star cooling models.

The general relativistic effects introduce several corrections to the equations of motion of the fluid and also to the formulae of neutrino heating rate due to the redshift and bending of neutrino trajectory. We found that these corrections increase entropy and decrease dynamic time scale of the expanding neutrino-driven wind from those in the Newtonian case. The most important corrections among them proves to be the correction to the hydrodynamic equations. Both temperature and density of the relativistic wind decrease more rapidly than the Newtonian wind as the distance increases without remarkable change of the velocity at $r < 30\text{km}$, where the neutrino-heating takes place efficiently. The lower the temperature and density are, the larger the net heating rate is. This is the main reason why the entropy in the relativistic case is larger than the Newtonian case.

We also looked for suitable environmental condition for the r-process nucleosynthesis in general relativistic framework. We studied first the differences and similarities between relativistic and Newtonian winds in numerical calculations, and then tried to interpret their behavior by expressing gradients of the temperature, velocity and density of the system analytically under the reasonable approximations. We

extensively studied the key quantities for the nucleosynthesis, *i.e.* the entropy S and the dynamic time scale τ_{dyn} of the expanding neutrino-driven wind, and their dependence on the protoneutron star mass, radius, and neutrino luminosity. We found that more massive or equivalently more compact neutron star tends to produce explosive neutrino-driven wind of shorter dynamic time scale, which is completely different from the result of the previous studies in the Newtonian case which adopted approximation methods. We also found that the entropy becomes larger as the neutron star mass becomes larger. Since the larger luminosity makes the dynamic time scale shorter, the large neutrino luminosity is desirable as far as it is less than 10^{52}ergs/sec . If it exceeds 10^{52}ergs/sec , only the mass outflow rate becomes large and the flow can not cool down to $\sim 0.2\text{MeV}$ by the shock front $r \sim 10,000\text{km}$. As the result, the time scale becomes too long, which is not favorable to the r-process nucleosynthesis.

Although we could not find a model which produces very large entropy $S \sim 400$ as suggested by Woosley et al.(1994), it does not mean that the r-process does not occur in the neutrino-driven wind. We compared our results with Hoffman's condition and found that the short dynamic time scale $\tau_{dyn} \sim 6\text{ms}$, with $M = 2.0 M_{\odot}$ and $L_{\nu} = 10^{52}\text{ergs/sec}$, is one of the most preferable condition for producing r-process elements around the third peak ($A \sim 195$). In order to confirm this, we carried out numerical calculations of the r-process nucleosynthesis upon this condition by using fully implicit single network code which takes account of more than ~ 3000 isotopes and their associated nuclear reactions in large network. We found that the r-process elements around $A \sim 195$ and even the heavier elements like thorium can be produced in this wind, although it has low entropy $S \sim 130$. The short dynamic time scale $\tau_{dyn} \sim 6\text{ms}$ was found to play the role so that the few seed nuclei are produced with plenty of free neutrons left over at the beginning of the r-process. For this reason the resultant neutron-to-seed ratio, $n/s \sim 100$, is high enough even with low entropy and leads to appreciable production of r-process elements around the second($A \approx 130$) and third ($A \approx 195$) abundance peaks and even the hill of rare earth elements between the peaks.

Note that the energy release by the interconversion of nucleons into α -particles at $T \sim 0.5\text{MeV}$ produces an additional entropy about $\Delta S \sim 14$. This

was not included in our present calculation. We can make note that, taking account of this increase, the r-process could occur in the neutrino-driven wind from hot neutron star whose mass is smaller than $2.0M_{\odot}$.

One might think that short τ_{dyn} brings deficiency of neutrino heating and that the wind may not blow. It is not true because the mass elements in the wind are heated by energetic neutrinos most efficiently at $r \lesssim 30km$, while the expansion time scale τ_{dyn} is the time for the temperature to decrease from $T \sim 0.5$ MeV to 0.2 MeV at larger radii. The duration of time for the mass elements to reach 30km after leaving neutron star surface is longer than τ_{dyn} . There is enough time for the system to be heated by neutrinos even for τ_{dyn} as low as ~ 6 ms.

We did not include neutrino-capture reactions that may change Y_e during the nucleosynthesis process. Since the initial electron fraction was taken to be relatively high $Y_e = 0.4 \sim 0.5$, there is a possibility that the final nucleosynthesis yields in neutrino-driven wind may be modified by the change in Y_e during the α - and r-processes. However, this is expected to make a small modification in our present expansion model with short dynamic time scale because the typical time scale of neutrino interaction is longer than τ_{dyn} . We will report the details about the nucleosynthesis calculation including neutrino-capture reactions in forthcoming papers.

It was found that the entropy decreases with increasing neutrino luminosity. This fact suggests that one cannot obtain large entropy by merely making the heating rate large. The cooling rate, on the other hand, does not depend on the neutrino luminosity. In the present studies we included two cooling mechanisms of the e^+e^- capture by free nucleons and the e^+e^- pair annihilation. As for the cooling rate due to the e^+e^- pair annihilation, only the contribution from pair-neutrino process is usually taken into consideration, as in the present calculation. However, there are many other processes which can contribute to the total cooling rate. They are the photo-neutrino process, the plasma-neutrino process, the bremsstrahlung-neutrino process and the recombination-neutrino process (Itoh, Hayashi, & Nishikawa 1995). Indeed, if we double our adopted cooling rate artificially, we can obtain larger entropy. Details on the numerical studies of the cooling rate are reported elsewhere. The radial dependence of the heating rate is also important (Qian & Woosley 1996). Since both heating and cooling processes are critical to deter-

mine the entropy, more investigation on the neutrino process is desirable.

There are other effects which have not been included in the present study. They are, for example, the mass accretion onto the neutron star, the time variation of the neutrino luminosity, convection and mixing of materials, and rotation or other dynamic process which break spherical symmetry of the system. These probably important effects may make several modifications to the present result. However, we believe that our main conclusion that there is a possibility of finding the r-process nucleosynthesis in an environment of relatively small entropy and short dynamic time scale is still valid. We conclude that the neutrino-driven wind is a promising astrophysical site for the successful r-process nucleosynthesis.

We are grateful to Prof. G.J. Mathews and Prof. J. Wilson for many useful discussions and kind advice. We also would like to thank Profs. R.N. Boyd, S.E. Woosley, H. Toki, Drs. K. Sumiyoshi, S. Yamada, and H. Suzuki for their stimulating discussions. This work has been supported in part by the Grant-in-Aid for Scientific Research (1064236, 10044103) of the Ministry of Education, Science, Sports and Culture of Japan and the Japan Society for the Promotion of Science.

REFERENCES

- Anders, E. and Grevesse, N. 1989, *Geochim. Cosmochim. Acta* 53, 197
- Bethe, H.A. 1990, *Rev. Mod. Phys.*, 62, 801
- Bethe, H.A. 1993, *ApJ*, 412, 192
- Bethe, H.A., Applegate, J.H., and Brown, G.E. 1980, *ApJ*, 241, 343
- Bethe, H.A. and Wilson, J.R. 1985, *ApJ*, 295, 14
- Burbidge, E.M., Burbidge, G.R., Fowler, W.A., and Hoyle, F. 1957, *Rev. Mod. Phys.*, 29, 547
- Burrows, A., & Mazurek, T.J. 1982, *ApJ*, 259, 330
- Cardall, C.Y. and Fuller, G. 1997, *ApJ*, 486, L111
- Cowan, J.J., Thielemann, F.-K., and Truran, J.W. 1991, *Phys. Rep.*, 208, 267
- Duncan, R., Shapiro, S.L., and Wasserman, I. 1986, *ApJ*, 309, 141

- Hillebrandt, W. 1998, in Proc. Int.Sympo.on Numerical Astrophysics, ed. S.Miyama, T.Hanawa, and T.Tomisaka, in press
- Hillebrandt, W., Takahashi, K., and Kodama, T. 1976, A&A, 52, 63
- Hoffman, R.D., Woosley, S.E., and Qian, Y.-Z. 1997, ApJ, 482, 951
- Ishimaru, Y., and Wanajo, S. 1999, ApJ, 511, L33
- Itoh, N., Hayashi, H., and Nishikawa, A. 1995, AAS CD-ROM series, vol.5
- Käppeler, F., Beer, H., and Wisshak, K. 1989, Rep. Prog. Phys., 52, 945
- Kodama, T. and Takahashi, K. 1975, Nucl. Phys. A, 239, 489
- McLaughlin, G.C., Fuller, G.M., and Wilson, J.R. 1996, ApJ, 472, 440
- Meyer, B.S. 1995, ApJ, 449, L55
- Meyer, B.S., Mathews, G.J., Howard, W.M., Woosley, S.E., and Hoffman, R.D. 1992, ApJ, 399, 656
- Meyer, B.S., McLaughlin, G.C., Fuller, G.M. 1998, Phys. Rev. C58, 3696
- Qian, Y.Z., Haxton, W.C., Langanke, K., and Vogel, P., 1997, Phys. Rev. C55, 1532
- Qian, Y.Z., and Woosley, S.E. 1996, ApJ, 471, 331
- Seeger, P.A., Fowler, W.A., and Clayton, D.D. 1965, ApJS, 11, 121
- Shapiro, S.L. & Teukolsky, S.A. 1983, in Black Holes, White Dwarfs, and Neutron Stars (New York: John Wiley & Sons, Inc.)
- Shen, H., Toki, H., Oyamatsu, K., and Sumiyoshi, K. 1998, Nucl. Phys. A, 637, 435
- Snedden, C., McWilliam, A., Preston, G., Cowan, J.J., Burris, D.L., and Armoski, B.J. 1996, ApJ, 467, 819
- Sollerman, J., Cumming, R.J., and Lundqvist, P. 1998, ApJ, 493, 933
- Sumiyoshi, K., Yamada, S., Suzuki, H., and Hillebrandt, W. 1998, A&A, 334, 159
- Surman, R., Engel, J., Bennett, J.R., and Meyer, B.S. 1997, Phys. Rev. Lett. 79, 1809
- Symbalisty, E., and Schramm, D. 1982, Astrophys. Lett., 22, 143
- Takahashi, K., Witt, J., and Janka, H.-Th. 1994, A&A, 286, 857
- Takahashi, K., and Janka, H.-Th. 1996, in Proc. Int. Sympo. on Origin of Matter and Evolution of Galaxies (Atami, Japan), eds. T.Kajino, S.Kubono & Y.Yoshii (Singapore: World Scientific), 213
- Thieleman, F.-K. Private communication, 1995
- Turatto, M., et al. 1998, ApJ, 498, L129
- Wilson, J.R. 1998, private communication.
- Witt, J., Janka, H.-Th., and Takahashi, K. 1994, A&A, 286, 842
- Woosley, S.E. and Hoffman, R.D. 1992, ApJ, 395, 202
- Woosley, W.E., & Weaver, T.A., 1993, in Supernovae: les Houches Summer School, Vol.54, ed. S.Bludman, R.Mochkovitch, & J. Zinn-Justin (Amsterdam: North Holland)
- Woosley, S.E., Wilson, J.R., Mathews, G.J., Hoffman, R.D., and Meyer, B.S. 1994, ApJ, 433, 229
- Wrean, P.R., Brune, C.R., and Kavanagh, R.W. 1994, Phys. Rev. C49, 1205
- Yamada, S., Janka, T.-H., and Suzuki, H. 1998, astro-ph/9809009, submitted to A&A

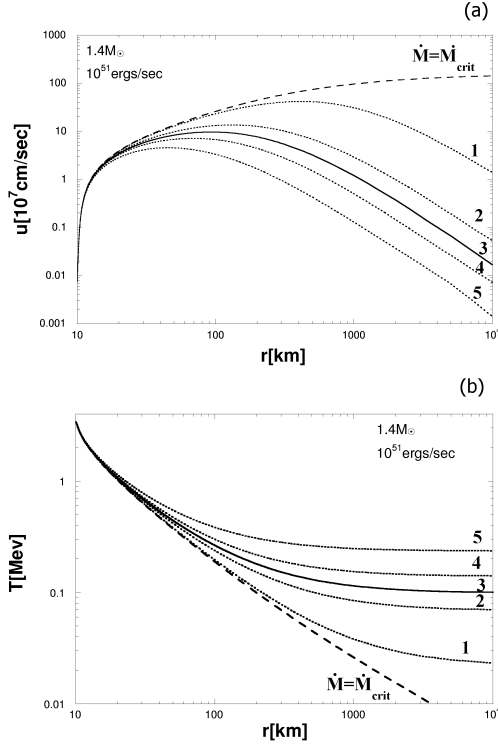


Fig. 1.— Outflow velocity (a) and temperature (b) in Schwarzschild geometry as a function of the distance r from the center of the neutron star for various mass outflow rate \dot{M} , where neutron star mass $M = 1.4 M_\odot$ and neutrino luminosity $L_{\nu_e} = 10^{51}$ ergs/s are used. Long dashed curve is for the critical mass outflow rate $\dot{M}_{\text{crit}} = 5.2681 \times 10^{-6} M_\odot$, in which the velocity becomes supersonic through the critical point. Fives curves denoted by 1 to 5 corresponds respectively to $\dot{M} = 5.25 \times 10^{-6}$, 5.15×10^{-6} , 5.0855×10^{-6} , 5.0×10^{-6} , and $4.8 \times 10^{-6} M_\odot$. Calculated result denoted by “3” meets with our imposed boundary condition of $T = 0.1$ MeV at $r = 10000$ km. Entropy per baryon S and dynamic timescale τ_{dyn} , which correspond to each curves from 1 to 5, are tabulated in Table 1. Note that the temperature denoted by “5” does not decrease to $T = 0.5/e$ MeV within 10000 km (see Table 1).

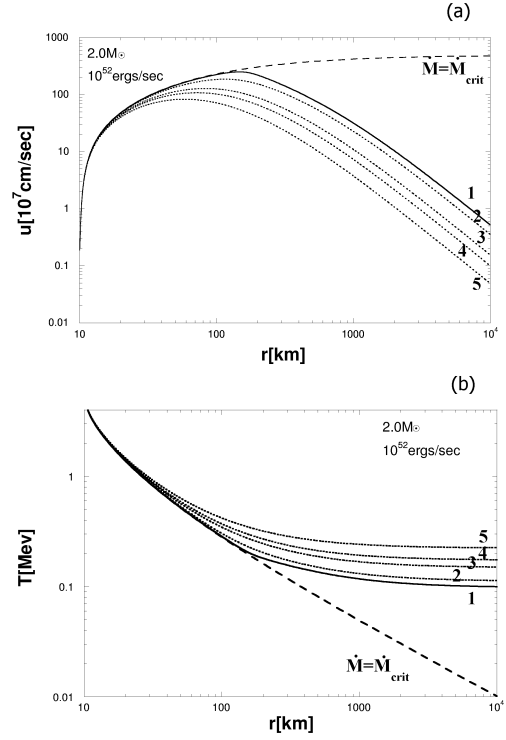


Fig. 2.— The same as those in Fig.1, for the case of $M = 2.0 M_\odot$, $L_{\nu_e} = 10^{52}$ ergs/s. Long dashed curve is for the critical mass outflow rate $\dot{M}_{\text{crit}} = 1.2459 \times 10^{-4} M_\odot$, and fives curves denoted by 1 to 5 correspond respectively to $\dot{M} = 1.245 \times 10^{-4}$, 1.240×10^{-4} , 1.225×10^{-4} , 1.215×10^{-4} , and $1.195 \times 10^{-4} M_\odot$. Calculated result denoted by “1” meets with our imposed boundary condition of $T = 0.1$ MeV at $r = 10000$ km. Entropy per baryon S and dynamic timescale τ_{dyn} , which correspond to each curves from 1 to 5, are tabulated in Table 1. Note that the temperature denoted by “5” does not decrease to $T = 0.5/e$ MeV within 10000 km (see Table 1).

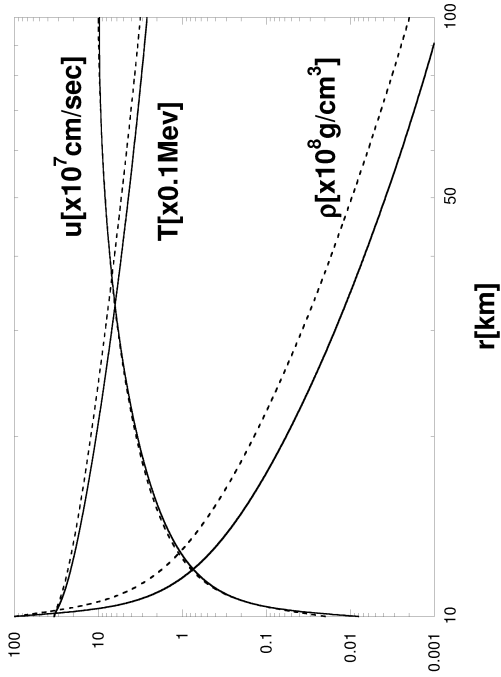


Fig. 3.— Outflow velocity $u(r)$, in unit of 10^7 cm/sec , temperature $T(r)$, in unit of 0.1 MeV , and baryon mass density $\rho_b(r)$, in unit of 10^8 g/cm^3 , as function of the distance r from the center of the neutron star with the protoneutron star mass $M = 1.4 M_\odot$, radius $R = 10 \text{ km}$, neutrino luminosity $L_\nu = 10^{51} \text{ ergs/s}$ and initial density 10^{10} g/cm^3 . Solid and broken lines display the results in Schwarzschild and Newtonian geometries, respectively. We choose the mass outflow rate $\dot{M} = 5.0855 \times 10^{-6} M_\odot/\text{s}$ for the Schwarzschild case and $\dot{M} = 1.2690 \times 10^{-5} M_\odot$ for the Newtonian case. See text for details of the outer boundary condition on \dot{M} .

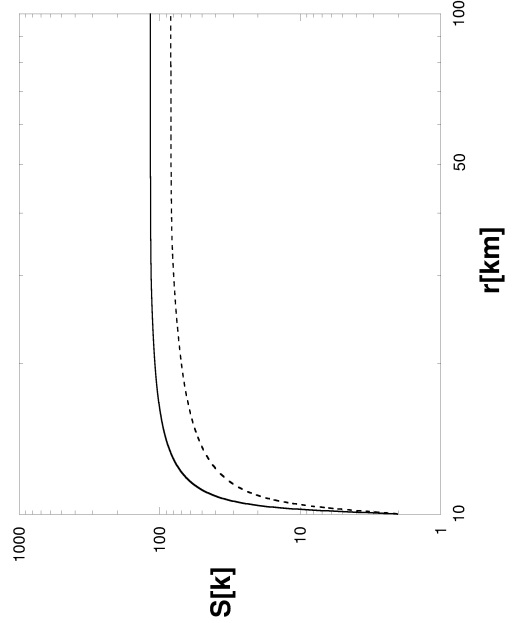


Fig. 4.— Entropy per baryon $S(r)$ as a function of the distance r from the center of the neutron star. Solid and broken lines are the same as those in Fig. 1 for the same set of the input parameters.

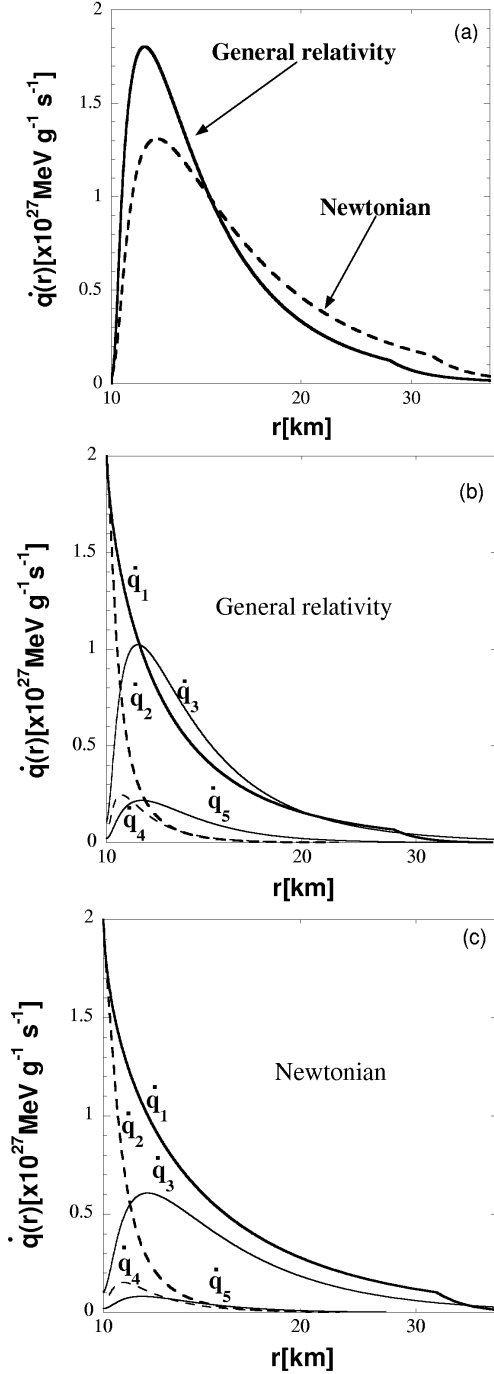


Fig. 5.— Specific neutrino heating rate $\dot{q}(r)$ as a function of the distance r from the center of the neutron star, for the same set of the input parameters as those in Fig. 1. (a) Total net heating rate \dot{q} . The solid and broken lines are for the Schwarzschild (denoted by general relativity) and Newtonian case, respectively. (b) Decomposition of the net heating rate into five different contributions from the heating process \dot{q}_1 , \dot{q}_3 , and \dot{q}_5 (solid lines) and the cooling process \dot{q}_2 and \dot{q}_4 (broken line) for the Schwarzschild case. See text for details of \dot{q}_i . (c) The same as those in (b) for the Newtonian case.

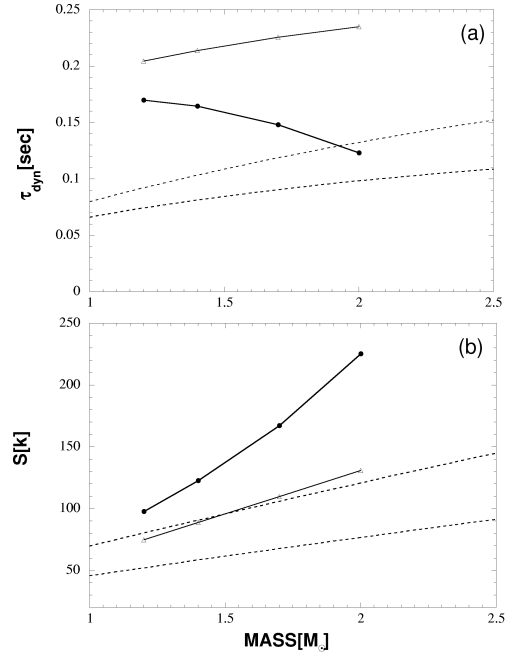


Fig. 6.— Dynamic time scale τ_{dyn} (a) and entropy per baryon S (b) vs. neutron star mass M at 0.5 MeV . Closed circles, connected by thick solid line, and open triangles, connected thin solid line, are the calculated results for the Schwarzschild and Newtonian case, respectively, by using the same set of the input parameters as in Fig. 1. Two broken lines are from Qian and Woosley (1996) in Newtonian case, which adopted an assumption of the radiation dominance (lower in τ_{dyn} , and upper in S) or the dominance of non-relativistic nucleon (upper in τ_{dyn} , and lower in S).

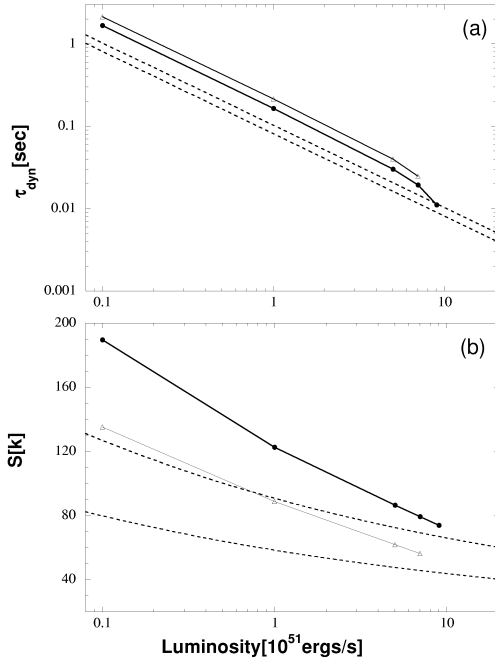


Fig. 7.— Dynamic time scale τ_{dyn} (a) and entropy per baryon S (b) vs. neutrino luminosity L_ν at $T = 0.5$ MeV. Thick and thin lines and two broken lines are the same as those in Fig. 4. At the larger end of $L_\nu \sim 10^{52}$ ergs/s, there is no solution to satisfy our imposed boundary condition, $T = 0.1$ MeV at $r = 10000$ km. See text details.

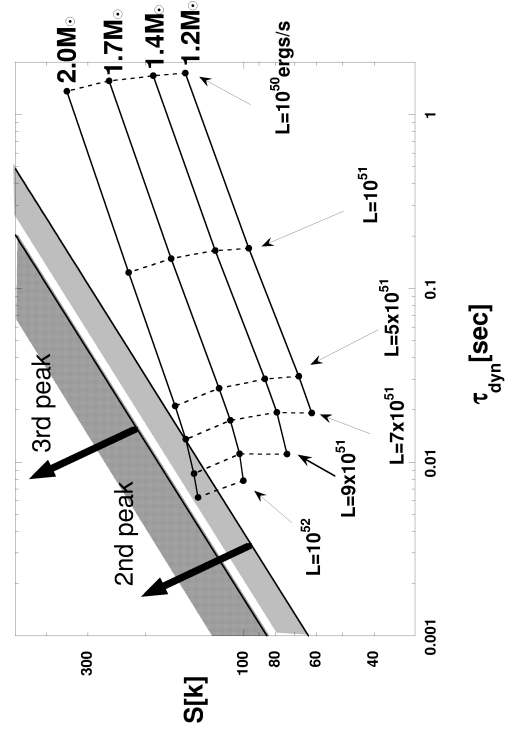


Fig. 8.— Relation between entropy per baryon S and dynamic time scale τ_{dyn} for various combinations of the neutron star mass $1.2M_\odot \leq M \leq 2.0M_\odot$ and the neutrino luminosity $10^{50} \leq L_\nu \leq 10^{52}$ ergs/s. Solid and broken lines connect the same mass and luminosity. At the largest end of $L_\nu \sim 10^{52}$ ergs/s for each M , there is no solution to satisfy our imposed boundary condition, $T = 0.1$ MeV at $r = 10000$ km. Two zones indicated by shadows satisfy the approximate conditions, for $Y_e = 0.4$, on which the successful r-process occurs (Hoffman et al. 1997) to make the second abundance peak around $A = 130$ (lower) and the third abundance peak around $A = 195$ (upper). See text for details.

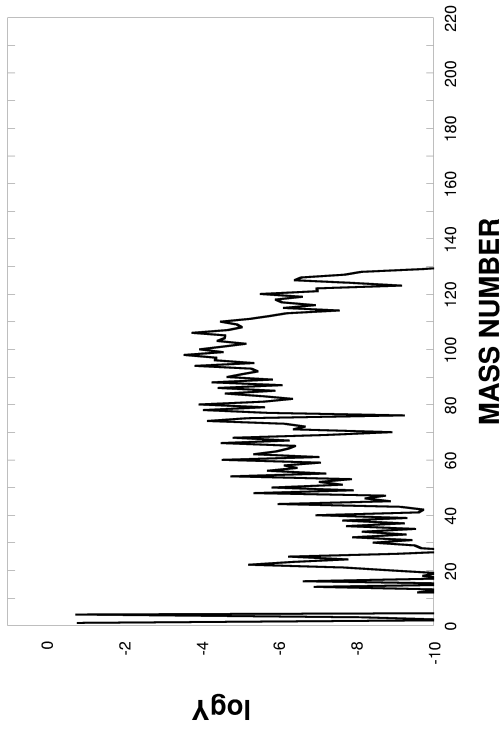


Fig. 9.— Seed abundances at $T_9 = 2.5$ as a function of atomic number A . See text for details.

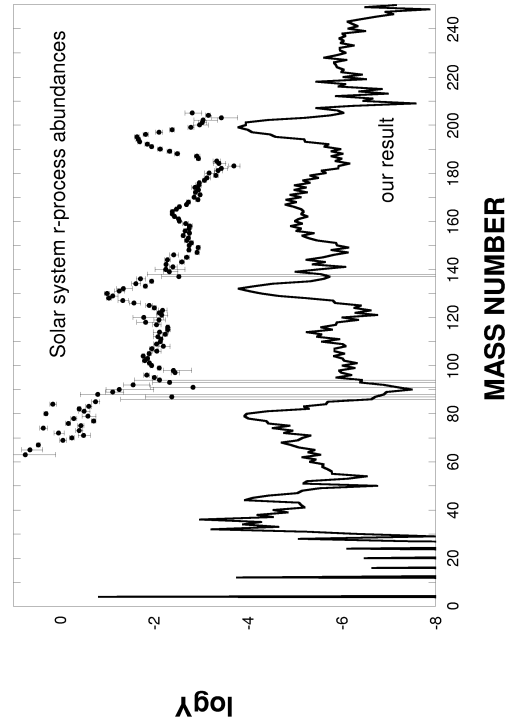


Fig. 10.— Final r-process abundances (lines) as a function of atomic mass number A compared with the solar system r-process abundances (filled circles) from Käppeler, Beer, & Wisshak (1989). The solar system r-process abundances are shown in arbitrary unit. See text for details.

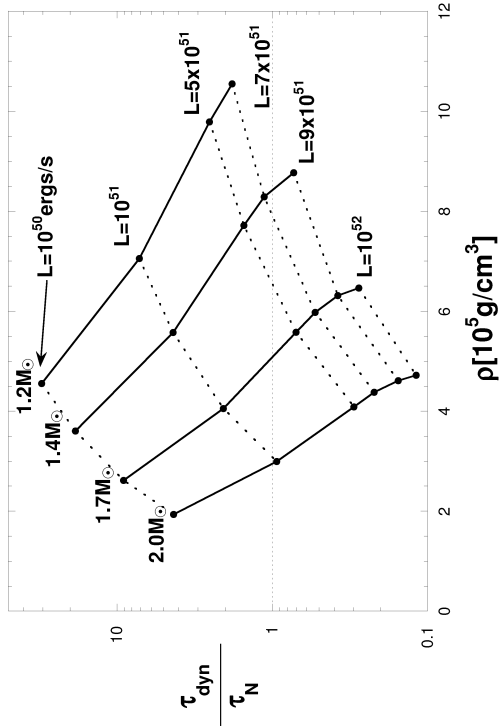


Fig. 11.— The ratio of dynamic time scale τ_{dyn} to the time scale of typical α -process nuclear reaction τ_N , τ_{dyn}/τ_N , vs. baryon mass density at $T = 0.5$ MeV, for various combinations of the neutron star mass $1.2M_\odot \leq M \leq 2.0M_\odot$ and the neutrino luminosity $10^{50} \leq L_\nu \leq 10^{52}$ ergs/s. Solid and broken lines connect the same mass and luminosity.

TABLE 1

ENTROPY AND DYNAMIC TIME SCALE FOR DIFFERENT \dot{M} . SINCE THE TEMPERATURE IN THE 5TH CASE FOR BOTH $M = 1.4M_{\odot}$ AND $M = 2.0M_{\odot}$ DOES NOT DECREASE TO $T = 0.5/\epsilon$ MEV WITHIN 10000 KM, τ_{dyn} IS NOT DEFINED (SEE FIG. 1(B) AND 2(B)).

| | | \dot{M} ($10^{-6}M_{\odot}/\text{sec}$) | entropy (k) | τ_{dyn} (s) |
|--------------------------------------|-------------------|--|--------------------|--------------------------------|
| $1.4M_{\odot}, 10^{51}\text{ergs/s}$ | M_{crit} | 5.2681 | 116 | 0.037171 |
| | 1 | 5.2500 | 117 | 0.041304 |
| | 2 | 5.1500 | 120 | 0.084335 |
| | 3 | 5.0855 | 123 | 0.16455 |
| | 4 | 5.0000 | 126 | 0.71569 |
| | 5 | 4.8000 | 135 | |
| $2.0M_{\odot}, 10^{52}\text{ergs/s}$ | M_{crit} | 1.2459×10^2 | 138 | 0.00507 |
| | 1 | 1.2450×10^2 | 138 | 0.00618 |
| | 2 | 1.2400×10^2 | 139 | 0.01088 |
| | 3 | 1.2250×10^2 | 141 | 0.08962 |
| | 4 | 1.2150×10^2 | 143 | 2.6272 |
| | 5 | 1.1950×10^2 | 146 | |